6

Multicolor Luminescence from Semiconductor Nanocrystal Composites Tunable in an Electric Field

G.N. Panin
[1]*Department of Physics, Quantum-Functional Semiconductor Research Center Dongguk University, Seoul,*
[2]*Institute of Microelectronics Technology & High Purity Materials, Russian Academy of Sciences, Chernogolovka,*
[1]*Korea*
[2]*Russia*

1. Introduction

Semiconductor nanostructures have interesting electro-optic properties due to quantum confinement of electrons, strong exciton binding energies, and the possibility to tailor the bandgap and radiative emission rates. An electric field normal to the quantum well, for example, shifts the absorption edge to lower energies (red-shift) and increases the refractive index below the absorption edge allowing to control the intensity of a light beam through electroabsorption. Such nanostructures can be conveniently used for the direct modulation of light, since they show much larger electro-optic effects than bulk semiconductors. Moreover, the optical properties of semiconductor nanostructures can be controlled by an electric field due to different emission rates from radiative centers in different charge states.

In the Chapter, the effect of an external electric field on cathodoluminescence from semiconductor nanocrystals and nanocomposites with different radiative emission rates is described, giving special emphasis to ZnO nanocrystals in MgO and polymer matrix.

In the next Section we shortly review the preparation of ZnO nanocrystals and nanocomposites, including a chemical solution deposition (CSD) of core/shell nanocrystals, as well as their structural and optical properties.

In Section 3 of the chapter, the effect of an external electric field on cathodoluminescence from the nanocrystal/polymer structure will be studied, giving special emphasis to the doped ZnO nanocrystals in Poly(4,4'- diphenylene diphenylvinylene) (PDPV) matrix and PBET/ITO structures. Electric field-induced color switching of cathodoluminescence from nanocrystals/polymer is reviewed. The assumed mechanism of electric field-tunable cathodoluminescence implies the presence of radiative recombination channels, which are sensitive to the electric field through the band bending at the crystal surface. The experiments on a reversible quenching of the UV near-band-edge emission under visible

illumination confirm an appearance of the recombination channel after recharging oxygen-vacancy states in the surface depletion zone. It has been shown that the UV near-band-edge emission can be modulated at frequencies of hundreds of hertz. Limiting performance bounds for potential future devices fabricated from nanocrystals with different radiative emission rates are considered.

2. Structural and optical properties of ZnO (MgO) nanocrystals and nanocomposites

Zinc oxide is a II-VI compound semiconductor with a wide direct band gap of 3.3 eV at room temperature (RT), which makes it attractive for optoelectronic devices in the near UV region (Kang et al., 2006; Look, 2001; Özgür et al. 2005). ZnO has a large exciton binding energy of about 60 meV, which promises efficient RT exciton emission. The unique physical and electronic properties of ZnO, such as large bond strength and large damage threshold for laser irradiation, (Minne et al., 1995; Yamamoto et al., 1999) and its high exciton binding energy allow to fabricate an excitonic laser operating at room temperature (Bagnall et al., 1997; Ohtomo et al., 2000; Yu et al., 1997). A lower pumping threshold for laser operation is expected when exciton-related recombination rather than electron–hole plasma recombination occurs. The use of a ZnO-based quantum structure with a higher exciton binding energy could decrease significantly the current threshold, which is the key point for current injection laser. The modified density of states in the ZnO-based low-dimensional quantum structure can confine both excitons and photons, thus achieving high-efficiency stimulated emission (Sun et al., 2000). The RT cathodoluminescence (CL) spectrum of ZnO along with the exciton emission band at near 380 nm contains a deep-level defect related emission band at 500–650 nm. The deep-level emission band, as usual, is considered consisting of the green (500–520 nm), yellow-orange (560– 600 nm), and red (650 nm) bands. The green emission band is frequently observed and the early studies it was attributed to copper impurities (Özgür et al., 2005). However at present, oxygen vacancies have been assumed to be the most likely candidate for recombination centers involved in the green luminescence of ZnO (Cheng et al., 2006; Leiter et al., 2001; Studenikin et al., 1998b; VanDijken et al., 2000a; Vanheusden et al., 1996a, 1996b). UV (exciton) and visible (defect) emissions are in competition with each other and it is presumed that the deep level emission centers are preferable channels of the electron-hole recombination. Such behavior of the luminescence bands gives rise to interesting physical phenomena, which creates an ability to control the intensity of the UV emission, and could be also of practical relevance. In practice the dependence of the excitonic band on external and internal perturbations is widely used to modulate its intensity. The modulations of the excitonic PL by means of acoustic (Takagaki et al., 2003), terahertz waves (Klik et al., 2005) and visible light (Chen et al. 1996; Shih H. Y. et al., 2011; Kurbanov et al., 2008a; Kurbanov et al., 2008b) as well as the excitonic PL and CL by electrical field (Hagn M., et al., 1995; Panin et al., 2005a; Schmeller et al., 1994; Zhang S. K., et al., 2001; Zimmermann et. al., 1997; Zimmermann et al., 1998; Zimmermann et al., 1999) were reported. The opportunity to control the characteristics, in particular, reflectance, of the sample under study by the external periodic perturbations serves as a basis for the modulation spectroscopy and allow to study electron states and features of the semiconductor band structure (Aigouy et al., 1997; Motyka et al., 2006; Rowland et al., 1998). In ZnO nanocrystals the electron paramagnetic-resonance signal assigned to singly ionized oxygen vacancy (V_0^+) was observed to be photosensitive for photon energies down to as low

as 2.3 eV (Vanheusden et al., 1996a, 1996b). Upon illumination, the V_0^+ density was observed to grow. Moreover, it has been found that the intensity of the green emission in ZnO powder correlates well with the paramagnetic single-ionized oxygen-vacancy (V_0^+) density. Nevertheless, the effect of the subband excitation on emission from ZnO is still unclear and remains unexplored in spite of the observed correlation between the density of V_0^+ and the green emission intensity and the sensitivity of V_0^+ to a visible light.

MgO (E_g = 7.3-7.7 eV) (Roessler & Walker, 1967; Johnson, 1954) solved in ZnO can produce a large band gap $Mg_xZn_{1-x}O$ alloy, which is well suitable for quantum structures operating in the ultraviolet spectral range (Ohtomo et al., 1998; Sharma et al., 1999). The radiative recombination of electron–hole pairs in terms of the quantum confined Stark effect was observed in ZnO/$Mg_xZn_{1-x}O$ structures (Makino et al. 2002). According to the phase diagram of ZnO/MgO binary systems (Raghavan et al., 1991), the thermodynamic solid solubility of MgO in a ZnO matrix is less than 4 mol%. The crystal structure of ZnO (hexagonal, a = 3.24 Å and c = 5.20 Å) is vastly different from that of MgO (cubic, a = 4.24 Å). However, since the ionic radius of Mg^{2+} (0.57Å) is almost the same as that of Zn^{2+} (0.60 Å) (Shannon, 1976), Zn^{2+} can be replaced by Mg^{2+} in the ZnO matrix. The synthesis of cubic $Mg_xZn_{1-x}O$ nanocrystals under pressure was reported (Baranov et al., 2005a; Baranov et al., 2010). Stable cubic $Mg_xZn_{1-x}O$ solid solutions *(*$0.33 < x < 0.68$*)* with continuous band gap up to 3.74 eV have been synthesized under high pressures and high temperatures.

2.1 The growth techniques

The growth techniques of NCs are very important since they influence their structure, shape and distribution of nanocrystal sizes, stoichiometry, structure of the surfaces or interfaces, and their optical properties. Therefore, before studying in the next sections the electric field induced optical properties of NCs, we want first to briefly look to the chemical growth techniques, paying special attention to the techniques of self-assembling (Fu et al, 2003; Fu et al., 2005; Panin et al., 2003b; Panin et al 2004d; Panin et al., 2005c; Panin et al., 2007d; Kurbanov et al., 2008c) as well as structural and luminescent properties of as-grown and annealed NCs. Nanostructuring by *physical techniques* based on lithography and etching does not usually produce NCs of sizes small enough for the detection of size effects, even if one uses electron beam techniques. The advantage of these techniques is their compatibility with microelectronics techniques. However, the drawback top / bottom of lithographic techniques in their low productivity and poor optical quality of structures produced by etching. The *chemical techniques* are the ones most used for the preparation of NCs. We will mention a few of them which have been used in preparation of ZnO-based composites.

2.1.1 Colloidal synthesis of ZnO nanoparticles

Colloidal synthesis, by the reduction of metal salts in solutions with organic ligands, are frequently used to produce metal nanoclusters (e.g. gold). As for II-VI semiconductors, nanoparticles of ZnO, CdSe, CdS, etc. are produced from reagents containing the nanocrystals constituents. One reagent contains the metal ions (e.g. Zn^{2+}) and the other provides the oxygen (O^{2-}) or the chalcogenide (e.g. Se^{2-}). The size of the nanocrystals is controlled by the temperature of the solutions and the concentrations of the reagents and the stabilizers. Synthesis of ZnO nanoparticles with sizes of 2–8 nm is fairly detailed, (Baranov

et al., 2008; Sakohara et al., 1998; Van Dijken et al., 2001; Wong et al., 2001; Meulenkamp, 1998; Pesika et al., 2003; Spanhel & Anderson, 1991; Tokumoto et al., 2003; Hosono et al., 2004) and the conditions for nanoparticle manufacturing by precipitation of zinc acetate with alkali from alcoholic solutions are also well studied. In particular, particle growth rate curves were obtained and the effects of several factors were determined, such as the water proportion in the solution, the nature of the solvent, the starting solution concentration, and precipitation temperature.

A typical absorption spectrum from suspended ZnO nanoparticles is shown in Fig 2.1 The simplest way to estimate the particle size in colloidal ZnO solutions is to determine the transition position in optical absorption spectra. The absorption onset of ZnO nanocrystals appears at 337nm, which is blueshifted relative to 382 nm absorption onset of bulk ZnO. The spectrum shows that these uncapped ZnO nanoparticles were well dispersed in ethanol, and that the band gap absorption was much more effective compared to the absorption by surface defect states (Chen et al., 1997).

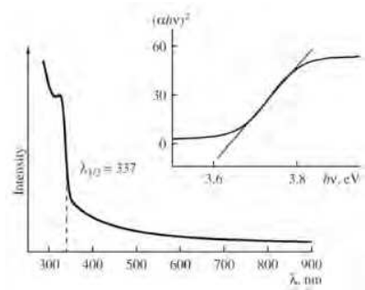

Fig. 2.1. Optical absorption spectra of colloidal ZnO particles prepared in ethanol. In the inset, the same data in other coordinates. (Baranov et al., 2008)

The inset in Fig. 2.1 illustrates the experimental data in the $(\alpha h\nu)^2 - h\nu$ coordinates. The existence of a linear segment on the $(\alpha h\nu)^2$ versus $h\nu$ curve verifies the existence of a direct electron transition which defined the particle adsorption edge. Extrapolation of this segment to axis $h\nu$ gave a value of 3.6 eV for the band gap of suspended ZnO nanoparticles. Compared to the band gap of micron-sized ZnO (E_g = 3.3 eV), the band gap of ZnO nanoparticles was increased by the quantum confinement effect. The method which we used is to equate E_g with the wavelength at which the absorption is 50% of that at the excitonic peak (or shoulder), so called $\lambda_{1/2}$. To convert measured values of $\lambda_{1/2}$ into particle size an expression (1) can be used:

$$1240/\lambda_{1/2} = a + b/D^2 - c/D \quad (1)$$

where $\lambda_{1/2}$ in nm, diameter D in Å and the values a= 3.556, b =799.9, and c = 22.64, which gives a good description of the experimentally found size dependence for 25 < D < 65 Å (Meulenkamp, 1998). The mean particle size calculated using expression 1 was ~3.0 nm. Comparison of the data derived from the absorption spectra with TEM data and theoretical calculations demonstrates good convergence.

ZnO nanoparticles synthesized from aqueous solution (Kurbanov et al., 2007a; Wang et al., 2005) and deposited on a substrate show usually the larger size (100-1000 nm) and cone-shape (Fig. 2.2 (a)).

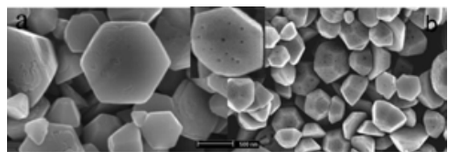

Fig. 2.2. Typical SEM images of ZnO nanocrystals (a) as-prepared and (b) annealed in air at 500 °C. The inset shows the specklike defects revealed after annealing at higher magnification. (Kurbanov, et al., 2009a)

As-prepared ZnO nanocrystals display a strong UV luminescence accompanied with a weak yellow–orange emission at around 565 nm. With increasing the excitation power a violet PL band at ~400 nm starts to appear and it dominates over the UV near-band-gap emission at high excitation power. While the UV–PL band intensity displays saturation behavior, the violet band intensity grows superlinearly. The violet luminescence most likely arises from defects associated with zinc vacancy or zinc vacancy related complexes.

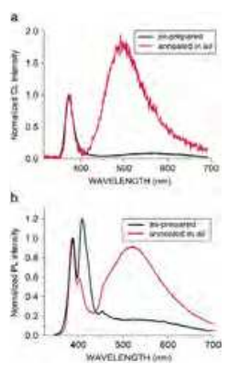

Fig. 2.3. Normalized (a) CL and (b) PL spectra of ZnO nanoparticles: (black) as- prepared and (red) after annealing in air at 500 °C for 1h. (Kurbanov et al., 2009b)

Figs. 2.3 (a) and (b) show the normalized room temperature CL and PL spectra of the ZnO nanoparticles before and after annealing in air at 500 °C for 1h, respectively. The annealing resulted in a strong increase in intensity of the green band centered at 505 and 520 nm in the CL and PL spectra, respectively. This band became dominant emission band in the visible region. The decrease in intensity of the violet band at ~400 nm after annealing is clearly observed in the spectra obtained at the high laser power excitation (80 mW) (Fig. 2.3 (b)). The UV emission from nanocrystals is ascribed to near-band- edge luminescence of ZnO. The variation of the UV peak energy as a function of temperature described by the Varshni equation also confirms this statement (Kurbanov et al., 2009b). Because the ZnO nanocrystals were prepared without intentional doping, the violet, green and yellow–orange emissions are attributed to native defect centers and their complexes. Namely, the yellow–orange emission band around 560–580 nm from the as-prepared ZnO nanocrystals has been assigned to oxygen interstitial related defects. The green band peaked at 505–520 nm appearing after the high-temperature annealing and being dominant in the visible emission is attributed to oxygen vacancy related centers. The observed differences in the green band positions in CL and PL spectra could be attributed to specific features of photon and electron beam excitation, particularly, to a different penetration depth of photons and electrons. The first principles investigations show that under oxygen-rich conditions the zinc

vacancy and oxygen interstitials are the dominant defect types and they have low formation enthalpies than other defects (Erhart et al., 2006; Kohan et al., 2000). Based on these calculations, it is reasonable to suggest that the violet emission from ZnO nanocrystals grown in thermal equilibrium conditions is originated from Zn vacancy related defects or their complexes. Moreover, as was mentioned above, in most cases the violet emission band is accompanied with the yellow–orange band, attributed to oxygen interstitials (Kumar et al., 2006; Hua et al., 2007; Jeong et al., 2003; Wu et al., 2001; Zhao et al., 2005;). The first principles studies predict that for Zn vacancy, the transition level (0 /-1) lies at ~0.45 eV (Kohan et al., 2000) or ~0.3 eV (Erhart et al., 2006) above the valence band and the transition level (-1/-2) is located at ~0.8 eV (Kohan et al., 2000) or 0.7eV (Erhart et al., 2006) above the valence band. Thus a transition between the conduction band and the single charged Zn vacancy acceptor level would give rise to luminescence at 405 nm (3.06 eV), in reasonable agreement with the predicted transition energy.

A postgrown annealing treatment significantly improved the UV emission efficiency and resulted in the clear appearance of a low temperature emission band around 3.31 eV (so-called A-line). Spatially and wavelength resolved CL measurements revealed a spotlike distribution of the A-line emission on a nanocrystal surface with a strong correlation between the emission around 3.31 eV and the specklike defects that appeared on the nanocrystal surface after annealing. At low temperatures, bound exciton emissions from ZnO nanocrystals are the dominant radiative recombination channels. The energy range between 3.375 and 3.367 eV is normally assigned to ionized donor bound excitons, while the neutral donor bound excitons are positioned between 3.366 and 3.36 eV. The free exciton emission is usually observed at 3.377 eV. According to the conventional classification for the bulk ZnO crystals, the lines situated at lower energies, between 3.33 and 3.31 eV, are attributed to the two-electron satellite (TES) recombination of the donor bound excitons (Kang et al., 2006; Meyer et al., 2004; Teke et al., 2004). However, in recent years many research groups reported on an observation of a strong emission line in the TES region the so called A-line. The position of the A-line varies from 3.31 to 3.333 eV depending on the growing methods of ZnO. The A-line's intensity is strongly enhanced in ZnO powders when compared to bulk ZnO (Fallert et al., 2007). The origin of the A-line emission is currently under discussion. Possible assignments of the A-line include: neutral excitons bound to nitrogen impurities (Look et al., 2002; Yang et al., 2006), donor-acceptor pair recombination (Zhang et al., 2003), free-to neutral- acceptor transitions (Cao et al., 2007), two-electron transition of exciton bound to neutral donor (Studenikin et al., 2000), the first longitudinal optical (LO) phonon replica of free excitons (Hirai et al., 2008) or excitons bound to surface or structural defects (Fallert et al., 2007; Fonoberov et al., 2006; He et al., 2007; Meyer et al., 2004; Teke et al., 2004). Recently, on a basis of cathodoluminescence measurements, it was suggested that this line is composed of two overlapped bands related to point defects and the first LO phonon replica of the free exciton (Mass et al., 2008).

Wavelength resolved CL images as well as, spatially resolved CL spectra from ZnO nanocrystals show a direct correlation between the A-line emission at 3.311 eV and the annealing induced specklike defects (Kurbanov et al., 2009a). The specklike defects appear on all faces of the annealed nanocrystals and lead to a spotlike distribution of the emission. Figure 2.3 (b) shows a SEM image of the annealed ZnO nanocrystals. The annealing of the nanocrystals leads to the formation of specklike defects on their surface, which appear as dark spots and are not observed on the as-prepared nanocrystal faces.

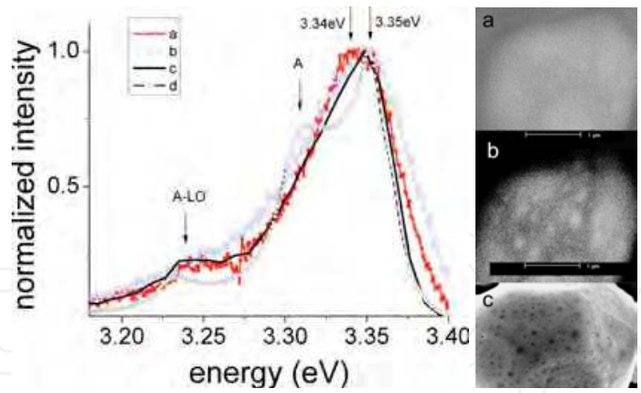

Fig. 2.4. (Left) Spatially resolved CL (a, b) and integral CL(c) and PL (d) spectra at 90 K. Spatially resolved CL measurements were performed on ZnO nanocrystal face: specklike defect region (a) and defect-free region (b); (Right) Wavelength resolved CL images of the ZnO nanocrystal face obtained at 90 K for (a) 3.358 eV (DX-line) and (b) 3.313 eV (A-line) energies as well as a SE image of the ZnO nanocrystal face with specklike defects (c).

The spatially resolved CL spectra, as well as, the integral PL and CL spectra obtained from a large number of ZnO nanocrystals at 90 K are presented in Fig. 2.4. It can be seen that in contrast to the PL spectrum the DX and A-lines in the integral CL spectrum are not well resolved; whereas, the A-LO line at around 3.24 eV appears clearly [Fig. 2.4, curve (c)] The spatially resolved CL spectrum from the nanocrystal surface region without specklike defects peaks at 3.35 eV; it is broadened and displays no A-LO line [Fig 2.4, curve (b)]. A spectral maximum of the CL spectrum from the specklike defect region is redshifted and located at 3.34 eV [Fig. 2.4 (a).] Moreover, it shows the pronounced A-LO peak at around 3.24 eV. Obviously, the A and A-LO lines appear only in the CL spectra collected locally from the regions with the specklike defects, or a large number of nanocrystals with the specklike defects. Fig. 2.5 shows the wavelength resolved CL images taken at the DX (3.358 eV) and A-line (3.311 eV) energies at 90 K. The CL image monitored at the bound exciton energy exhibits an uniform distribution and no extraordinary features are observed [Fig. 2.4 (a)]. In contrast, the emission detected at the A-line energy is spotlike and localized [Fig. 2.4 (b)]. The distribution of the spots coincide with position of the specklike defects in the secondary electron image [Fig. 2.4 (c)].

2.1.2 ZnO nanorods

Numerous techniques have recently been developed to synthesize quasi-1D ZnO nanostructures, (Baranov et al. 2004; Liu et al., 2004; Xia et al., 2003; Yang et al., 2002; Yao et al., 2002; Yin et al., 2004; Wang et al., 2004; Zhang et al., 2003) including growth with or without catalysts by a vapour–liquid– solid epitaxial (VLS) mechanism (Yang et al., 2002; Yao et al., 2002; Wang et al., 2004), microwave plasma growth (Zhang et al., 2003) and solution methods (Liu et al., 2004; Yin et al., 2004). An important issue in the fabrication of nanostructures is the control of the shape and size of nanomaterials, both of which affect their optical and electrical properties. ZnO nanorods grown from a NaCl ($NaCl–Li_2CO_3$) salt mixture were described by (Baranov et al., 2005b; Baranov et al. 2004). The salt composition and the size of the Zn-containing precursor particles play a key role in the synthesis and define their size and properties.

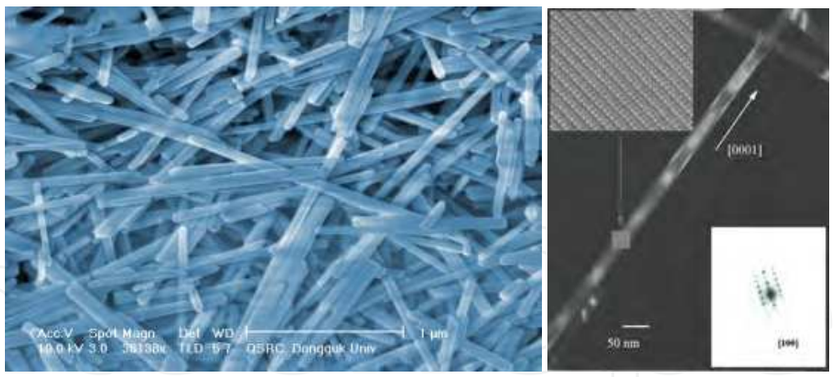

Fig. 2.5. (Left) HRSEM images of ZnO nanorods grown from the NaCl–Li_2CO_3 salt mixture at 700° C for 1 h and (Right) TEM images of ZnO nanorods grown from the NaCl mixture at 700° C for 1 h. Insets—selected area of electron diffraction and the ZnO atom-scale resolution image (HRTEM).

Figures 2.5 show HRSEM and TEM images of ZnO nanorods synthesized from the NaCl–Li_2CO_3 salt mixture as well as their selected area diffraction analysis. The presence of Li_2CO_3 allows to decrease the diameters of ZnO nanorods. The product prepared at 600° C for 3 h consists of quite uniform nanorods with diameters ranging from 8 to 40 nm and of length from 200 to 500 nm. As the temperature increased to 800° C, the diameters of the nanorods increased drastically and ranged from 200 to 500 nm. The results indicate that individual nanorods are single crystalline and possess the wurtzite structure (see the inset in figure 2.5, right).

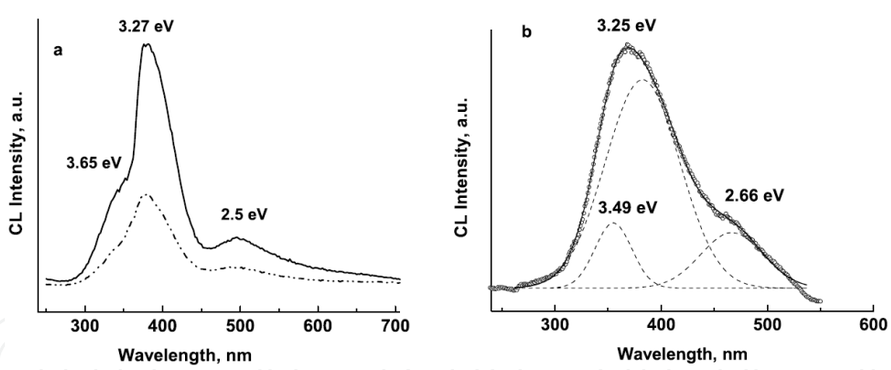

Fig. 2.6. (a) CL spectra taken at room temperature (V = 15 kV) from ZnO nanorods grown from (a) the NaCl mixture at 500° C (dash–dot line) and 700° C (solid line), (b) the NaCl–Li_2CO_3 salt mixture at 700° C (solid line) (the dashed lines are Gaussian multi-fit approximations) (Baranov et al., 2005b).

The CL spectra for the ZnO nanorods are shown in figure 2.6**.** Two peaks at around 3.25 eV and 2.5 eV and a high-energy shoulder at around 3.65 eV are observed. The high-energy bands 3.65 eV and 3.25 eV correspond to the near band-gap emission (NBE) of small and large rods, respectively. The high energy shoulder in the spectrum indicates some dispersion of small size rods. Strong quantum confinement effect could be attributed to the real size limitation by an potential barrier formed due to the charge surface states or the exciton dead layer (Pekar, 1958; Combescot et al., 2001), which increases with nanocrystal

size (Fonoberov et al., 2004). The UV shift of PL from nanocrystals which are large in comparison with the exciton Bohr radius in ZnO (~1 nm (Fonoberov et al., 2004; Gill et al., 2002)) has been reported. The UV NBE shift of about 40 meV was observed for surprisingly large (24 nm) ZnO nanocrystals (Hur et al., 2005).

2.1.3 CVD grown ZnO nanorods and tetrapods

Chemical vapor deposition (CVD) and vapor transport (VT) techniques are widely used for the growth of nanorods and tetrapods. The effect of growth conditions on their morphology, size and properties has been well studied (Lyapina et al., 2008) and high efficient light emitting diodes based on ZnO nanorods were reported (Lee et al., 2011).

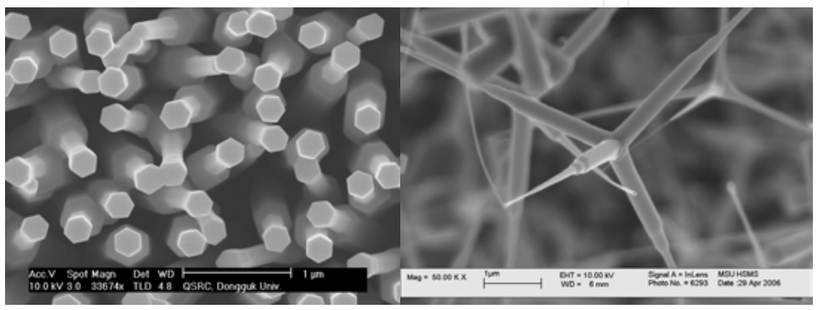

Fig. 2.7. SEM micrographs of ZnO nanorods and tetrapods grown on Si substrates.

Figure 2.7 shows typical ZnO nanostructures grown on a Si substrate. The supersaturation of the zinc vapor plays a key role in determining the morphology of the structures. The nanorods have a hexagonal shape and its size can be well controlled by the zinc vapor. The tetrapods are not bonded to the substrate surface, which implies that they were formed in the gas phase. The lower layer consists of small tetrapods with legs ~ 2–3 μm in length and ~ 350 nm in diameter. In the upper layer, the tetrapods have elongated legs on the order of 5μm in length, with a diameter of 650 nm at the junction and 100 nm at the tip. The rods of the tetrapods have long whiskers, up to 10 μm in length, with a sharp transition from a leg thickness of 500 to 80–100 nm.

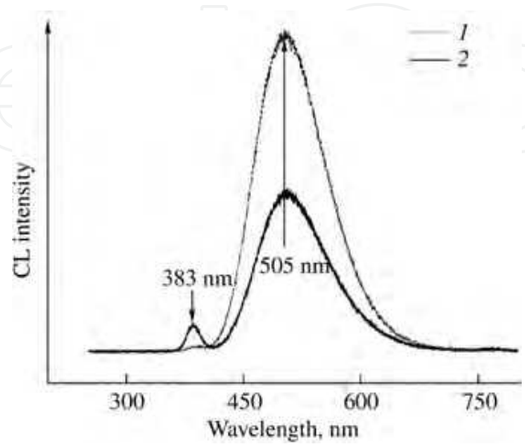

Fig. 2.8. CL spectra of tetrapods grown in (*1*) oxygen-deficient and (*2*) oxygen-enriched conditions (Lyapina et al., 2008).

Figure 2.8 shows the RT CL spectra of tetrapods obtained in different conditions. The UV peak at 383 nm is due to free excitons. The green band centered at 505 nm is markedly stronger. The intensity ratio between the UV and green emissions is larger in the samples obtained at the highest oxygen flow rate and reduced zinc vapor concentration.

2.1.4 ZnO/MgO nanocrystals and nanocomposites

The techniques for growing nanocrystals inside a matrix are very developed, partly as a consequence of the industrial production of color filters and photochromic glasses based on copper halides, such as CuCl, CuBr, CuI, etc. Nanocrystals of II-VI compounds (ZnO, CdS, CdSe, ZnSe, etc.), starting from supersaturated viscous solutions, are also frequently incorporated in glass matrices for applications in optical filters due to the ease in controlling the dot size. ZnO/MgO composites can be prepared by using aqueous solution and methanol solution techniques (Panin et al., 2004c; Panin et al., 2005b). Fig. 2.9 (Left) shows SEM images of the ZnO/MgO particles prepared by these techniques. The sizes of the individual ZnO and MgO particles prepared from the aqueous solution are approximately 100 and 500 nm, respectively, while the size of the particles prepared from the methanol solution is about 10 nm.

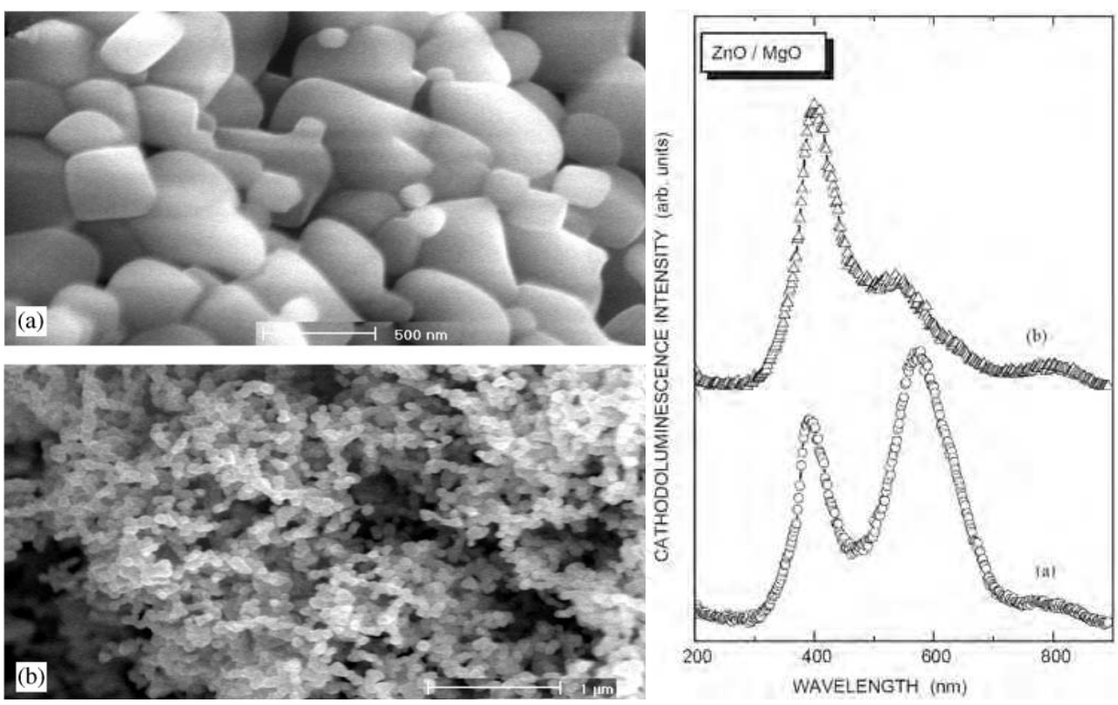

Fig. 2.9. (Left) Scanning electron microscopy images of ZnO/MgO nanoparticles prepared by using (a) aqueous solution and (b) methanol solution techniques. (Right) RT CL spectra of the ZnO/MgO particles annealed in (a) N_2 and (b) O_2 atmospheres.
(right panel) shows CL spectra of the large-size ZnO/MgO particles annealed in an oxygen or nitrogen environments. Annealing in oxygen environment inhibits the green luminescence and enhances the near-band-gap emission.

2.1.5 ZnO/MgO core-shell nanocrystals

ZnO/MgO core-shell nanocrystals were synthesized by chemical solution deposition (CSD) technique using a colloidal zinc oxide solution and alcoholic solution of magnesium acetate as described in (Baranov et al., 2008).

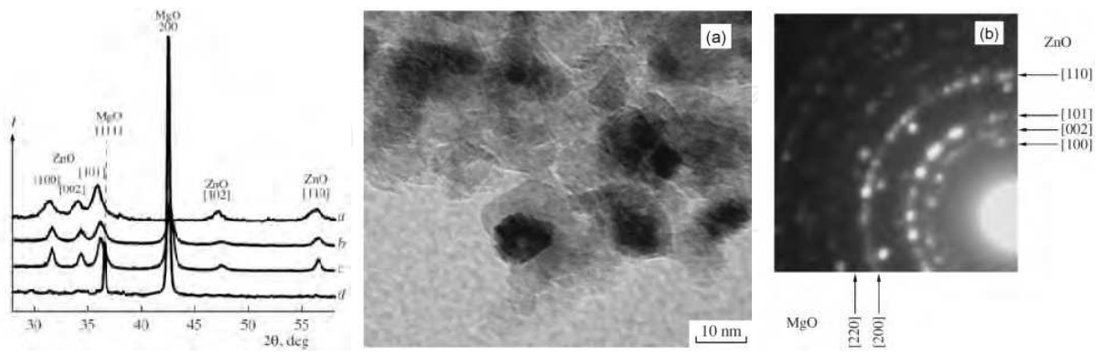

Fig. 2.10. XRD patterns from powdered nanoparticles of (*a*) ZnO annealed at 400° C and (*b*), (*c*), and (*d*) ZnO/MgO composites, annealed at 400, 500 and 600° C, respectively. (Right) (a) TEM micrograph and (b) electron diffraction pattern of the ZnO/MgO nanocomposite annealed at 500° C.

X-ray powder diffraction and electron diffraction show that, although the synthesis temperature was rather low, nanoparticles have a crystal structure. The XRD pattern of ZnO sample (Fig. 2.10, curve (a)) consistent with the hexagonal phase of ZnO crystals; the unit cell parameters insignificantly differ from literature data: a = 3.249 Å and c = 5.206 Å. The coherence length for zinc oxide determined from diffraction peak broadening agrees well with the particle size derived by digitizing TEM micrographs (Fig. 2.10, (image) (a)) and is within 5 − 12 nm. X-ray powder diffraction and TEM data for samples annealed at 400, 500, and 600°C indicate that the optimal temperature range for ZnO/MgO composite manufacturing is 400–500°C. The X-ray diffraction patterns contain both peaks associated with the cubic MgO structure (with Miller indices 111 and 200) and those associated with zinc oxide (wurtzite; indices 100, 002, 101, 102, and 110) (Fig. 2.10, curves *b* and *c*). These peaks are considerably broadened, but there is no anisotropy in directions 100 and 002; that is, particles have near-spherical shapes, which are also seen in TEM micrographs (Fig. 2.10, image (a)). The ZnO coherence length (crystallite size) in the composite with MgO varies as a function of synthesis parameters more widely than for pure zinc oxide; crystallite sizes range from 8 to 14 nm. The unit cell parameters calculated for MgO and ZnO phases almost coincide with the literature values; this means that, there is no noticeable interaction between magnesium and zinc oxides with solid solution formation at the low annealing temperatures. It confirms also by the electron diffraction pattern for the nanocomposite annealed at 500°C which contains both indices attributed to the cubic MgO structure ([220], [200]) and those associated with wurtzite zinc oxide ([100], [002], [101], and [110]) (Fig. 2.10, image (b)). A different situation is observed for samples annealed at 600°C (Fig. 2.10, curve *d*) or higher temperatures. In this case, wurtzite phases vanish and there are only peaks of newly formed solid solution $Mg_{1-x}Zn_xO$; the init cell parameters of the cubic phase increase systematically, which corresponds to a partial substitution of zinc ions (with a larger ionic radius) for magnesium ions.

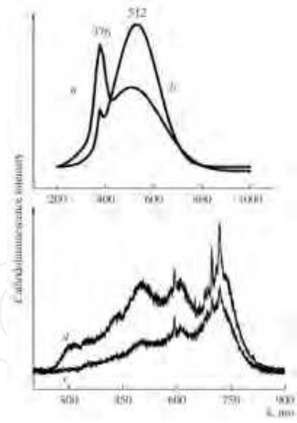

Fig. 2.11. Cathodoluminescence spectra of the ZnO/MgO nanocomposites annealed at (*a*) 400, (b) 500, (c) 600, and (d) 700° C (Baranov et al., 2008).

Cathodoluminescence spectra of annealed samples are shown in figure 2.11. The spectra of the samples annealed at 400 and 500°C show two peaks at 376 and 512 nm which are attributed to the free exciton luminescence and the oxygen-vacancy-related green emission from ZnO nanoparticles. The strong blue shift of the excitonic luminescence could be due to the quantum confinement effect in ZnO nanocrystals. The relationship between nanocrystal size and band gap can be obtained using a number of models (Efros & Rosen, 2000; Andersen et al., 2002; Hyberstsen, 1994). The effective mass model for spherical particles with a Coulomb interaction term (Brus, 1984; Brus, 1986) where the band gap E*[eV] can be approximated by Eq. 2 (Pesika et al., 2003):

$$E^*=E_g^{bulk}+[(\hbar^2\pi^2)/2er^2][(1/m_e m_0)+(1/m_h m_0)]-1.8e/4\,\pi\,\varepsilon\varepsilon_0 r, \quad (2)$$

where E_g^{bulk}=3.3 eV is the ZnO bulk band gap, r is the particle radius, m_e=0.26 is the effective mass of the electrons, m_h=0.59 is the effective mass of the holes, m_0 is the free electron mass, ε=8.5 is relative permittivity of ZnO, ε_0 is the permittivity of the free space, ħ is Plank's constant divided by 2π, and e is the charge of the electron. The size of the ZnO particles estimated from Eq. 2 was 8 nm that well agreed with TEM and X-ray diffraction data for the nanocomposites studied. The relative intensity of the green luminescence increases with an increase of annealing temperature (Fig. 2.11, curve b). This behavior of luminescence could arise from an increase in density of single-ionized oxygen vacancies after annealing as a result of an increase of the electron concentration in the ZnO particles. The spectra of the samples annealed at 600 and 700°C are shown in figure 2.11 (c, d). For the sample annealed at 600°C, edge luminescence is not observed but several peaks in green, yellow and red spectral regions are appeared. After annealing at 700°C, a peak in the deep UV region (at 307 nm) appears, confirming the formation of a solid $Mg_{1-x}Zn_xO$ solution, for which the UV shift of edge luminescence is characteristic. The peaks at around 600 and 700 nm can be attributed to Mg- or oxygen-related defects in the solid solution which together with oxygen vacancy defects reduces transparency of the nanocomposite in the visible range. The hexagonal ZnO (core) and cubic MgO (shell) phases in ZnO/MgO nanocomposites are thermally stable and high transparent up to 500°C. The annealing at temperatures 600 -700°C led to Mg doping and formation of the $Mg_{1-x}Zn_xO$ solid solution with the radiative defect centers, emitted in green, yellow and red spectral regions.

The luminescent properties of nanocomposite consisting of ZnO nanotetrapods (NT) and MgO particles were also investigated. The nanocomposites were prepared from ZnO tetrapods (300-5000 nm in length and 20-500 nm in diameter) grown by CVD method (Lyapina et al., 2008) and capped by MgO nanoparticles (3-50 nm) which were obtained by thermolysis of jellylike product containing mixture of magnesium acetate and sodium hydroxide alcohol solution (Baranov et al., 2008). The nanocomposite was annealed at 500°C in air. The low temperature annealing was used to prevent the diffusion of Zn^{2+} cations to MgO lattice and vice versa Mg^{2+} cations to ZnO lattice and keep the cubic MgO and hexagonal ZnO structures (Baranov et al., 2008; Panin et al., 2005b).

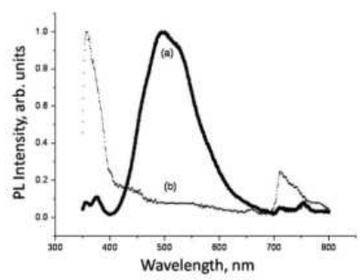

Fig. 2.12. The normalized PL spectra of (a) ZnO nanotetrapods (solid line) and (b) ZnO nanotetrapods covered by MgO (dot line).

Fig. 2.12 shows PL spectra of ZnO tetrapods and the tetrapods capped with MgO particles. The annealed tetrapods demonstrate high intensity of the green luminescence attributed to the oxygen-vacancy-related defects. The tetrapods annealed with capping MgO nanoparticles show however the suppressed green emission and the relatively-enhanced excitonic luminescence (Fig. 2.12, curve (b)). To study the electronic and optical properties of the samples on nano-scale through the lens detector (TLD) and CL measurements were carried out (Ryu et al., 2002; Panin et al., 2003a). Figure 2.13 (a) shows an HRSEM image of the tetrapod and (b) profiles of CL intensity and the TLD signal obtained from the structure by scanning an electron beam along the A-B line. The enhanced TLD signal indicates the electron depletion of a ZnO surface with formation of the space charge region. The intensity of CL from the depletion zone is suppressed significantly (about 25 %).

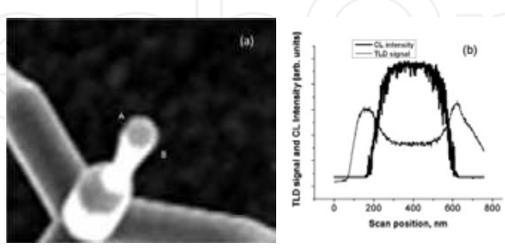

Fig. 2.13. (a) An HRSEM image of the nanotetrapod structure and (b) profiles of the CL intensity and the TLD signal from the structure obtained by an electron beam scanning (along the A-B line in (a)).

The green luminescence from ZnO nanocrystals are generally explained by the formation of single ionized oxygen vacancies (Vanheusden et al., 1996b). The mechanism of the observed suppression of the green luminescence from the nanocomposite structure could be

explained by the electron depletion of ZnO nanocrystals due to the band bending on the interface between ZnO and MgO capping agent. In the part of this depletion region where the Fermi level E_F passes below the V_0^+ /V_0^{++} energy level, all oxygen vacancies are in the nonradiative V_0^{++} state and the green luminescence from the nanocrystals is suppressed (Panin et al., 2008). In case of uncapped tetrapods the electron density is relatively high and the green emission from such samples is well appeared.

3. Tuneable luminescence from nanocrystals and composites

3.1 ZnO Nanocrystals capped by Rh6G

ZnO-based polymer and molecular composites have demonstrated the attractive optical and mechanical properties. In particular, it is found that capping of ZnO nanocrystals with polymer, organic dye, etc. can effectively passivate the surface defects and decrease the surface-related visible emission (Borgohain et al., 1998; Du et al., 2006; Harada et al., 2003; Tong et al., 2004; Yang et al., 2001). The remarkable increase of the near-band-edge emission to the visible emission intensity ratio (NBE/VB) in ZnO nanocrystals coated with Rhodamine 6G (Rh6G) organic dye was reported by (Kurbanov et al., 2007b). These results show that capping with Rh6G leads not only to passivation of the ZnO nanocrystals surface but also to formation of dye monomers mostly, due to advanced surface of ZnO nanocrystals.

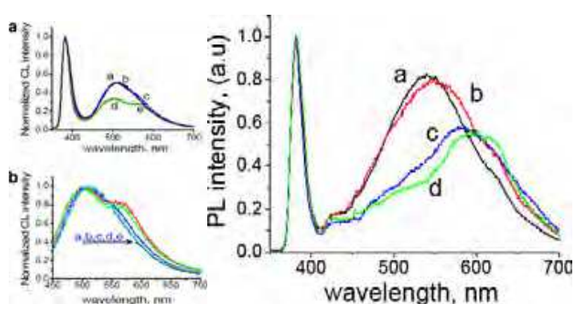

Fig. 3.1. RT normalized CL (Left) and PL (Right) spectra for ZnO nanocrystals impregnated with the various Rh6G concentration solutions: (Left) (a) uncapped, (b) 10^{-6} mol%, (c) 10^{-5} mol%, (d) 10^{-4} mol% and (e) 10^{-3} mol% and (Right) (a) uncapped, (b) 10^{-4} mol%, (c) 10^{-3} mol% and (d) 10^{-2} mol%. The spectra were normalized to (a) UV and (b) visible emission bands.

Fig. 3.1 shows the RT CL and PL spectra of ZnO nanocrystals impregnated with Rh6G solution of various concentrations. Both the CL and the PL spectra of the uncapped nanocrystals show two emission peaks – the sharp peak at 382 nm and a broad peak at ~510–530 nm. The luminescence at 382 nm is attributed to the near-band-edge emission (free exciton) and the broad emission peak at 510–530 nm is contributed to deep level defects, probably ionized charge states of oxygen vacancies (Studenikin et al., 1998b; VanDijken et al., 2000a; Van Dijken et al., 2001; Vanheusden et al., 1996a, 1996b). After capping with dye the emission spectra of ZnO nanocrystals display a new band at 560–570 nm. Its intensity increases with increasing dye concentration and it can be attributed to Rh6G luminescence. Moreover, at high dye concentrations a second band at 625 nm, which is also related to dye molecules, appears (Fig. 3.1 (right panel) d). However, the visible emission intensity around 510 nm decreases with increasing dye concentration and at higher dye concentrations, the

emission arisen from Rh6G becomes dominant over the visible luminescence of ZnO. The capping gave rise to increasing the intensity ratio of the UV emission to the visible emission of the ZnO nanocrystals. After capping, the (NBE/VB) intensity ratio for the CL spectrum increases from 1.96 to 3, and that for the PL spectrum increases from 1.22 to 3.6. Improvement of the (NBE/VB) intensity ratio indicates that dangling bonds and defect states in the surface layer of ZnO nanocrystals are significantly passivated by dye. The visible luminescence of ZnO nanocrystals located around 510–520 nm (''green'' emission) is affected by the surface (Matsumoto et al., 2002; Norberg & Gamelin, 2005; Ramakrishna & Ghosh, 2003; Shalish et al. 2004; VanDijken et al., 2000a; Van Dijken et al., 2001). A direct relationship between the size and the excitonic emission intensity in ZnO crystals in the 40–2500 nm size range was reported (Matsumoto et al., 2002; Shalish et al. 2004; Van Dijken et al., 2001). Moreover the ''green'' emission intensity was reported to display a direct correlation with surface hydroxide concentrations (Liu et al., 1992; Norberg & Gamelin, 2005; Van Dijken et al., 2000b). On the other hand, it has been found that surface OH groups can form H-bridges with dye molecules through their OH groups and/or nitrogen (Ying et al., 1993; Wood & Rabinovich, 1989). The evaporation of the residual ethanol solvent is accompanied with the increased interaction between dyes and hydroxides. Statistically neighboring molecules are bonded to the hydroxide groups, resulting in stabilization of dye molecules at the ZnO surface. The obtained results indicate that Rh6G molecules present as monomers at ZnO nanocrystals at lower dye concentrations. Fig. 3.2 shows PL spectra for the ethanol solutions containing Rh6G of 10^{-5}, 10^{-4}, and 10^{-3} mol%. The Rh6G solutions display only one PL band at ~560 nm resulting from monomers (Innocenzi et al., 1996). With increasing the dye concentration, this band exhibits redshift, which is attributed to formation of dimers and increasing their amount (Bojarski, 2002; Innocenzi et al., 1996). The aggregate formation process is clearly displayed in the PL spectrum of the dye deposited onto a flat quartz glass surface (Fig. 3.2 (curve d)). The PL spectrum contains peaks near 665, 625 and 530 nm. Using the results (Bojarski, 2002) we assume that the PL bands at 625 and 665 nm are formed due to dimer and aggregate emissions. The broad PL peak at 530 nm is related to the emission of the quartz glass. PL of organic dye on a quartz glass surface undergoes a strong quenching effect owing to strong aggregation and as a result, the dye emission intensity on the quartz glass surface is many orders of magnitude less then that in the ethanol solutions as well as on the ZnO nanocrystal surface.

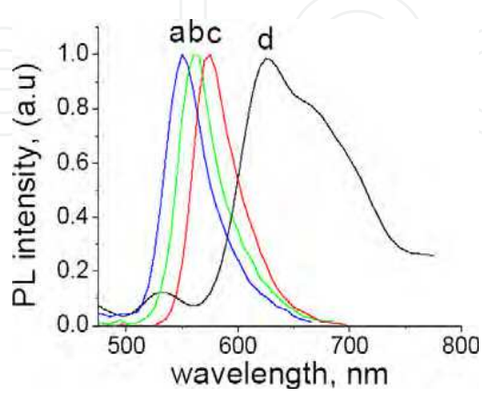

Fig. 3.2. Normalized PL spectra of Rh6G in ethanol solution for the different concentrations: (a) 10^{-5} mol%, (b) 10^{-4} mol%, (c) 10^{-3} mol% and (d) Rh6G deposited onto a flat quartz glass surface (Kurbanov et al., 2007b).

Based on these results, we can infer that the emission band at 625 nm appearing in the ZnO nanocrystal PL spectra at higher dye concentrations is caused by dimers and the spectrum redshift caused by increasing the dye concentration is evidence of the dimer formation process. However, the dye emission from the capped ZnO nanocrystals displays basically monomer-like behavior. The large surface to- volume ratio of nanocrystals contributes to isolating the dye molecules from each other that reduces the formation of dimers or complexes, especially at low dye concentrations. Similar behavior of materials with advanced surface structure to prevent the dye dimerization process has been observed in artificial opal (Kurbanov et al., 2007c), porous aluminum (Levitsky et al., 2002) and mesa structured titanium dioxide (Vogel et al., 2004) impregnated with dye. The dye covering the ZnO surface absorbs also the emission at around 500 nm. It is known that Rh6G has strong absorption bands near 500–530 nm and in the UV region (Bojarski, 2002; Ethiraja et al., 2005; Innocenzi et al., 1996). The findings indicate that the excitation of Rh6G at the surface of ZnO nanocrystals during our experiment may occur through two channels, which are an energy transfer from the ZnO deep level emission centers and a direct laser excitation. A significant increase in the suppression of the green luminescence appears at higher dye concentrations when the dimer related PL band at 625 nm has appeared. The Rh6G dimers have two absorption bands, higher intensity one at the short wavelength side of the monomer band (around 500 nm) and lower intensity one overlapping with the monomeric one at 560– 570 nm, which reabsorbs the emission of monomers. An increase of the dimer concentration might also lead to an increase in the absorption of the visible emission from ZnO nanocrystals and a decrease in the luminescence intensity from monomers. The surface passivation of ZnO nanocrystals due to the organic dye capping improved their UV-to-visible luminescence intensity ratio. Furthermore, a large surface area of nanocrystals helps to suppress the aggregate formation process of dye molecules, and Rh6G on ZnO nanocrystal surface displays a monomer-like emission, position of which depends on the dye concentration. The results indicate that ZnO nanocrystals capped with Rh6G organic dye hold promise for potential electro-optic applications.

3.2 CL from PBET structure

Organic semiconductors have the potential to provide a compact, low-cost light-emitting and laser diodes over a broad range of wavelength throughout the UV-visible spectrum. The large exciton binding energy in the conjugated polymers (Van der Horst et al., 2002) and efficient excitonic recombination can be the basis of high quantum yield devices operating at room temperature. Injecting electrons and holes into the charge states of the conjugated polymers leads to electroluminescence (Burroughes, 1990). These carriers should be balanced at the junction of the emitting layer to yield the maximum exciton formation. Light emission of poly [3-(2-benzotriazolo) ethylthiophene] (PBET) at a different electron beam current density has been investigated by the CL spectroscopy (Panin et al., 2004a). An electron beam was used to inject directly electrons and holes in the polymer and induced an electric field.

PBET was synthesized by (Ahn et al., 2001), to increase quantum efficiency by introducing benzotriazole, an electron-withdrawing moiety, to the thiophene. Singlet excitons are usually generated in polymer either by photoexcitation or by electrical injection of negative and positive charge carriers to the lowest unoccupied molecular orbital (LUMO) and the

highest occupied molecular orbital (HOMO), respectively. Due to large exciton binding energy and the lattice relaxation (Bredas et al., 1996) energy of photons emitted by polythiophene is usually significantly lower than the HOMO–LUMO band gap, which is around 3.58 eV (Van der Horst et al 2002). Both photoluminescence and electroluminescence spectra of the polymer show yellow–orange luminescence (Ahn et al., 2002).

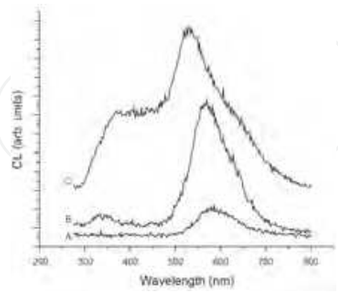

Fig. 3.3. CL spectra of PBET/ITO structure obtained at 10 kV accelerating voltage of incident electrons and at different electron beam current densities: (A) 0.4 A/cm^2, (B) 30 A/cm^2 and (C) 2 kA/cm^2 (Panin et al., 2004a).

Room temperature CL spectra of the PBET/ITO structure under various electron beam excitations are shown in Fig. 3.3. Under the low-excitation conditions with an incident beam current density of 0.4 A/cm^2 the spectrum (Fig. 3.4, A) is similar to the photoluminescence spectrum previously reported (Ahn et al., 2002). The peak centered at 580 nm with a shoulder at 620 nm were attributed to the π–π^* transition of the conjugated thiophene segments. Under higher excitation with a beam current density of 30 A/cm^2 (Fig. 3.3, B) three peaks centered at 340, 565 and 620 nm are revealed. Under the highest excitation used in our experiment with a beam current density of 2 kA/cm^2 the broad ultraviolet-blue bands are detected. In addition, a blue shift of green luminescence in the spectrum up to 529 nm and a red shift of the UV peak to 370 nm are observed. The peak at 347 nm could be attributed to the direct interband radiative transition. The absorption spectrum of the PBET samples has a strong absorption band at 282 nm (Ahn et al., 2002).

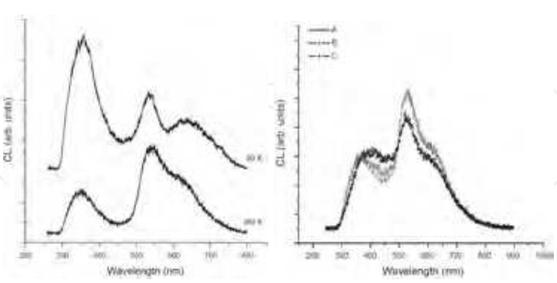

Fig. 3.4. (Left) CL spectra of the PBET/ITO structure acquired at 300 and 80 K at a 400 A/cm^2 electron beam current density. (Right) CL spectra of the structure obtained after the electron beam irradiation at the 400 A/cm^2 electron beam current density for different fluences: (A) 1.5×10^{21}, (B) 3.0×10^{21} and (C) 5.5×10^{21} cm^{-2}.

A relative intensity of the UV–blue band increases with increasing electron beam current density. Fig. 3.4 (Left) shows CL spectra of the PBET/ITO structure obtained under the high electron beam excitation at different temperatures. The UV band centered at 350 nm along

with green–orange luminescence bands are clearly observed. The relative intensity of the bands depends strongly on temperature. At 80 K the polymer structure shows the high intensity of the UV luminescence, which is substantially higher than that of the green–orange luminescence. Some red shift of a 620 nm peak is also observed. Note that no shifts for the UV band and no blue band appearances are detected under such excitation conditions. To investigate the origin of the blue band we measured the luminescence of the polymer structure after the electron beam irradiation with the high electron beam current density for various fluences and temperatures. As the fluence of the electron beam irradiation increases, the intensity of the broad violet–blue luminescence at 370–470 nm increases, while an intensity of the green–orange luminescence decreases (Fig. 3.4 (Right)). The blue–violet band is detected under room temperature excitation, but it has not appeared under the highest electron beam current density excitation at 80 K. The results indicate that the structural/electron change in the polythiophene derivative may occur under the room temperature electron beam irradiation with a high fluence. The most important observation is the appearance of UV and blue–violet emissions centered at 347 and 420 nm. The wide spectra with violet and UV emissions have been previously demonstrated in insulating polymers at high electric fields (Chayet et al. 1997; Massines et al., 1997). The high-energy photon emission in these systems was attributed to the so-called "impact ionization," which occurs when the injected and thermally generated carriers are accelerated by a strong electric field to cause collision excitations and subsequent radiative recombination. Theoretical models (Artbauer, 1996) suggest that the number of these collisions increases with electric field, which can be arisen from the electron beam induced charging. Our experimental results indicate that an increase of the electron beam current density results in charging of the polymer and an induced electric field which increases the UV CL intensity. The charging effect with formation of the built-in electric field in the polymer structure was clearly observed in a secondary electron mode and could be controlled by the electron beam current adjustment. The UV luminescence suggests the recombination of "hot" nonequilibrium carriers in the presence of the strong electric field. Impact excitation induced by the electric field produces a large number of excited carriers in excess of equilibrium ("hot" carriers). These excited states decay thus approaching their number at equilibrium via several competing mechanisms. Formation of singlet excitons, which decay radiatively emitting green luminescence, is one such possible mechanism. However, the strong electric field inhibits this type of decay by dissociation of the excitons, thereby enhancing the direct HOMO–LUMO interband radiative transition with UV emission. Under such conditions direct radiative transition is favorable over exciton recombination. The saturation of the green luminescence at high current density is a further evidence for the partial inhibition of exciton recombination. The appearance of the blue luminescence at high current densities could be due to the electron beam induced phase transformation in PBET at room temperature. When the polymer backbone conformations are coupled with that of the sidegroups the first-order phase transition is occasionally realized. Such polymers should show the bistable states, which are separated by a potential barrier in free energy. The phase conversion between the two states in some temperature region is thermally forbidden but may be possible by electron beam excitation. In the hysteretic temperature region of the phase transition the switching of the electronic phase was previously demonstrated by pulsed photoexcitation of electron-hole pairs in polythiophene (Hosaka et al., 1999). The photo-induced change in the absorption and luminescence spectra arising from the

structural change, which is generally termed photochromism, has been observed for many photochromic molecules with photoactive π-electron units and thin films of the semiconducting π-conjugated polymer (Koshihara et al. 1992). The structural change induced by the photoexcitation is considered to be minimal with least steric hindrance but significantly affects the π-conjugation length or the electronic structure. The photoexcited electron-hole pairs or their lattice relaxed analogs (polarons) are responsible as precursory excitations for the observed photoinduced phase transition. Origin of the blue luminescence from the polymer might be attributed to the electron beam induced change in the ring torsion angle by the interchain interaction in a substituted benzotriazole derivative segment.

Stimulated emission from the PBET/ITO structure in a broad range of wavelengths are observed at high current density (Panin et al., 2004b).

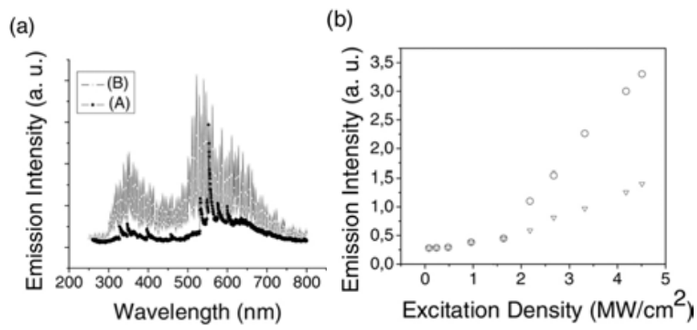

Fig. 3.5. a) RT spectra of stimulated emission (A) and lasing (B) from PBET obtained under electron beam excitation with different power densities: 1.5 MW/cm² (A) and 2 MW/cm² (B) and b) the intensity of emission as a function of the beam excitation density. (Panin et al., 2004b)

Figure 3.5 (a) shows RT spectra of stimulated emission (curve A) and multimode lasing in broad range of wavelengths (curve B) from the device structure obtained under electron beam excitation with high power densities. When the electron beam current density increases, the narrow emission lines appeared and the FWHM strongly decreases. A finely structured spectrum with features as narrow as 0.5 nm is observed at 2 MW/cm² power density. The narrow lines appear above a threshold power density and indicate stimulated emission. The dependence of the emission intensity on the pumping is shown in Fig. 3.5 (b). The broad spontaneous emission depends approximately linearly on excitation density. In contrast, stimulated emission shows the changeover to superlinear behavior. From the superlinear dependence we estimate an 1.3 MW/cm² threshold power density. The narrow lines appearing in the spectrum under high excitation are attributed to laser modes. These modes could be arising from self-assembled cavities formed in the polymer film due to recurrent light scattering (Cao et al., 1999) by domain boundaries. Small (10–20 nm) nanostructures in a fractal-like organization and elongated self-assembled aggregates of these structures forming extended domains (100–2000 nm) have been previously demonstrated in these polymer films using scanning tunneling microscopy and near-field optical measurements (Micheletto et al., 2001). It was shown that these structures are the source of the electroluminescence emission pattern which was observed due to domain boundaries scattering. Laser emission from these resonators results in a small number of discrete narrow peaks in the emission spectrum. As the pump power increases further, the gain increases and it exceeds the loss in the lossier cavities. Laser oscillation in those random cavities adds more discrete peaks to the emission spectrum.

3.3 ZnO Nanocrystal- PDPV composite

The combination of conjugated polymer and inorganic semiconductor nanoparticles is an attractive field in fabrication of light-emitting devices. Such nanocomposites allow combining the efficient luminescence from inorganic semiconductor with good mechanical and optical properties of polymer films (Friend et al., 1999; Vanheusden et al., 1996b). Poly(4,4'-diphenylene diphenylvinylene), (PDPV) (Eg=3.0 eV) (Feast et al., 1995) is a conjugated polymer for electroluminescence (EL) in the green region (Cacialli et al., 1997). The oxide semiconductor ZnO is a promising material for EL in the blue-UV region (Lee et al., 2011; Mordkovich et al., 2003; Panin et al., 2004c;). The luminescence efficiency of ZnO nanoparticles can be higher than that of ZnO epitaxial films and the particle-size dependent band gap allows controlling the excitation spectrum. ZnO nanocrystals doped by Mg, W, Fe, Mn, Y, Eu, V etc. show the high efficiency in multicolor low-energy CL and are prospective to use in advanced flat panel displays, solid state lighting applications and smart solid state electronics (Baranov et al., 2006; Mordkovich et al., 2003; Panin et al., 2007a; Panin et al., 2007b; Panin et al., 2007c).

PDPV (cis/trans~50:50) was prepared by condensation polymerization of 4,4'-dibensoyl–biphenyl following the procedure described elsewhere (Feast et al., 1995). The particles were prepared by dissolving the mixture of analytic-grade $ZnCO_3$ and $(MgCO_3)4Mg(OH)25H_2O$ (Aldrich) in a mole Zn/Mg ½ ratio in nitric acid and then precipitating by adding a $2M(NH_4)2CO_3$ solution. The precipitate was decomposed in a vacuum furnace at 320 °C and finally oxidized at 550 °C in air. The doping effect of ZnO by Mg has been observed after annealing of ZnO/MgO samples at temperatures above 500 °C (Panin et al., 2005b).This procedure leads to the formation of 12–60 nm sized Mg doped ZnO crystals (Panin et al., 2004c). PDPV was dissolved in chloroform and ZnO:Mg powder was dispersed in chloroform separately by treatment in an ultrasonic bath for 30 min. The PDPV mixed with the particles was deposited on a Si/SiO_2 substrate with gold electrodes separated by 5 µm by spin coating at 1000 rpm. The same procedure was used to get separate PDPV and ZnO:Mg particle films (Fig. 3.6).

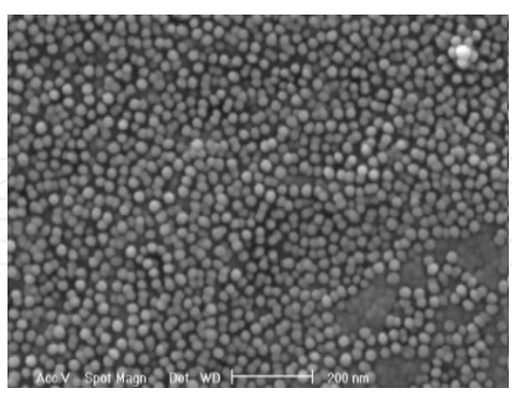

Fig. 3.6. An HRSEM image of the ZnO:Mg particle film (Panin et al., 2008).

Figs. 3.7 show CL spectra of the pristine PDPV film and the pristine ZnO:Mg particle film. PDPV has a well pronounced CL with the maximum emission in the green region, which is consistent with the luminescence results obtained for this polymer (Cacialli et al., 1997; Feast et al., 1995). The CL spectrum of ZnO:Mg nanoparticles reveals a more complicated structure with several peaks at 3.54; 2.83; 2.02 and 1.72 eV, respectively. The intensity of CL at 1.72 eV is higher

with respect to other picks, which indicates that the red emission from ZnO:Mg nanoparticles related to impurities or traps (Falcony et al., 1998; Studenikin et al., 1998a) is the dominant one.

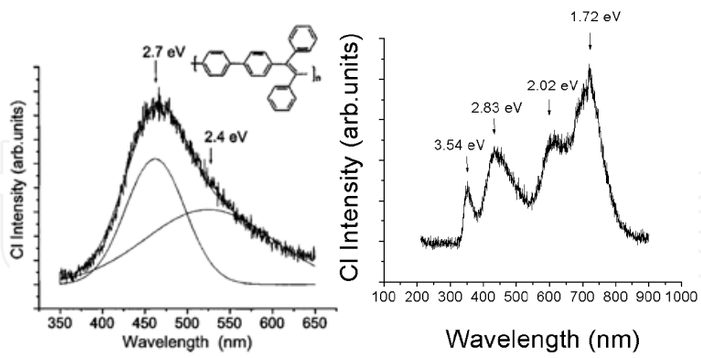

Fig. 3.7. CL spectrum of the PDPV film (Left) (inset shows chemical structure of PDPV) and the pristine ZnO:Mg particles (right).

3.3.1 Switching of cathodoluminescence from ZnO nanoparticle/polymer nanostructure by an electric field

The effect of reversible switching between blue-green and red emission in PDPV mixed with ZnO:Mg nanoparticles by an electric field was reported by (Panin et al., 2005a). Figure 3.8 (a) shows the CL spectrum of the PDPV–ZnO:Mg composite film without application of an electric field. The resulting spectrum combines CL from all the materials involved, which caused the broadening of PDPV spectrum with the pronounced peaks at 3.50, 2.86, and 1.79 eV. The main maximum of this asymmetric spectrum in the blue-green region (2.86 eV) results from pronounced blue-green emission from both PDPV and ZnO:Mg nanoparticles. As can be seen from Fig. 3.8 (b), application of a positive bias (+5 V) to the electrode suppresses the blue-green emission and shifts the emission maximum to the red region. The effect is found to be reversible with respect to the application of the electric field, namely then field was off, the emission maximum returned to the blue-green region.

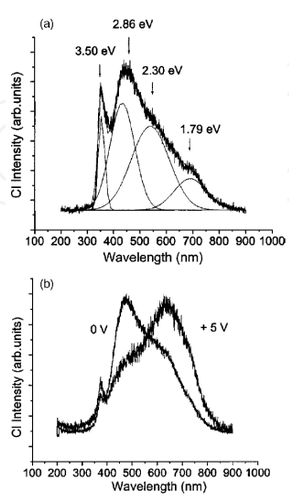

Fig. 3.8. CL of PDPV–ZnO:Mg composite film (a) without electrodes and (b) with electrodes biased with (+5 V) or without (0 V) application of an electric field (Panin et al., 2005a).

3.3.2 The mechanism of the electric field-tuneable luminescence from the ZnO nanoparticle/polymer structure

Before starting the analysis of the luminescence switching mechanism in PDPV–ZnO:Mg composite films, we have to note that the similar effect has been found in PPV films doped with ruthenium dinuclear complex (Welter et al., 2003). The band gap of ruthenium complex is about 0.5 eV smaller than that of the polymer. Therefore, the mechanism for the formation of the excited state in the polymer involves the ruthenium complex in a stepwise electron transfer process. In the case of the PDPV– ZnO:Mg composite the band gap of ZnO is higher than that of the polymer and the latter mechanism of the electric-field switching between blue-green and red emissions does not work (as well as the mechanism proposed for the emission from PPV–carbon nanotube composite (Woo et al., 2000). Fig. 3.9 shows the positions of the molecular orbitals and band structures of the materials used in our composite structure. As can be seen, there is a direct contribution to the green emission from LUMO-HOMO radiative recombination in PDPV and contributions to the blue, green and red emissions from radiative deep levels recombination in ZnO.

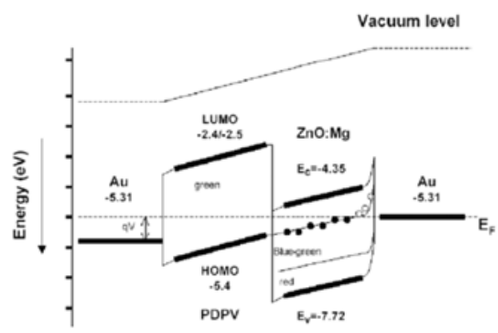

Fig. 3.9. Energy band diagram of a biased Au/PDPV/ZnO:Mg/Au structure (Panin et al., 2005a).

There are several models to explain the blue-green and red emission in ZnO. The most acceptable models assume that the defect centers responsible for green luminescence are the singly ionized oxygen vacancy centers (Vanheusden et al., 1996a, 1996b) or donor–acceptor level transitions (Egelhaaf & Oelkrug, 1996; Reynolds et al., 2001; Studenikin et al., 2002). The acceptor level (Zn vacancy) is located 2.5 eV below the conduction band edge (Bylander et al., 1978; Egelhaaf & Oelkrug, 1996), while the donor level (oxygen vacancy) is known as a shallow level at 0.05–0.19 eV, leading to an emission band centered around 508–540 nm. The blue-green emission in ZnO might also be associated with a transition within a self-activated center formed by a double-ionized zinc vacancy $(V_{Zn})^{-2}$ and the single-ionized interstitial Zn^{+} at the one or two nearest-neighbor interstitial sites (Studenikin et al., 1998c). At last the blue-green emission can be ascribed to a substitution of Zn by extrinsic impurities such as Cu or Mg in the crystal lattice (Dingle, 1969; Mordkovich et al., 2003). The blue-green emission in the doped ZnO particles can be attributed to recombination of $V_0^{\bullet}$ electrons with excited holes in the valence band (Fig. 3.10), while the red emission in the particles at 670 nm (E_d =1.84 eV) could originate from the complex defect-related centers such as deep donor and deep acceptor centers associated with V_{Zn} (Fig. 3.10) (Ohtomo et al., 1999; Studenikin et al., 1998b; Mitra et al., 2001).

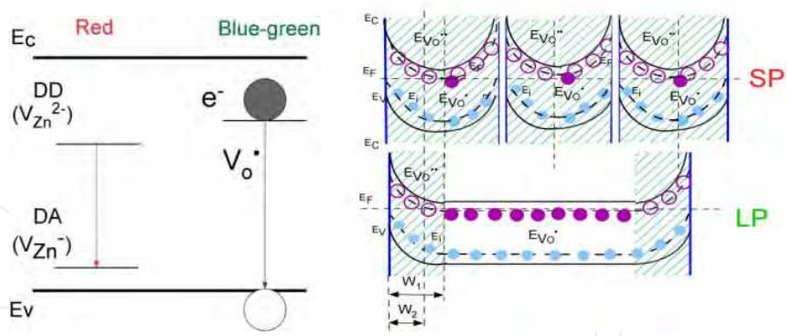

Fig. 3.10. (Left) Electron energy level diagram for red and blue-green radiation centers in ZnO. (Right) The energy-band diagrams of small (SP) and large (LP) particles in cross-sections.

The mechanism for the formation of the excited states in the PDPV–ZnO:Mg composite structure implies the presence of channels of radiative recombination, which can be controlled by electric field. Figure 3.10 (right panel) shows the energy-band diagrams for small (SP) and large (LP) particles in cross-sections. Application of an electric field causes depletion effects, which are known to affect the green luminescence of ZnO crystals (Vanheusden et al., 1996a; 1996b). A high density of electrically active surface states enhances the effect of band bending at a semiconductor surface, which creates an electron depletion region of width W in the particle. In the part of this region where the Fermi level E_F passes below the V_0^+ / V_0^{++} energy level, all oxygen vacancies are in the nonradiative V_0^{++} state. The CL maximum at ~2.86 eV indicates that both radiative recombination mechanisms including oxygen-vacancy related centers in ZnO and direct LUMO–HOMO transfers in PDPV coexist at zero electric field. It should be noted that band bending might be reduced by both polymer ZnO surface passivation and strong electron beam illumination. This effect results in an attraction of minority carriers to the surface, where they become trapped, and converts some of the V_0^{++} centers to the V_0^+ state. As for the red emission related to the recombination via impurity-oxygen involved centers in ZnO:Mg, the radiative recombination mechanism also works and can be recognized as the shoulder of the main spectra at ~650 nm. Complete band bending suppression at both interfaces in the case of the Au–PDPV–ZnO:Mg–Au structure can be obtained by applying a bias voltage to electrodes. PDPV is a *p*-type conductor similar to many other conjugated polymers. It means that application of positive bias to the Au–ZnO-PDPV increases the barrier and the green emission from PDPV is reduced because of charge separation at the polymer–nanocrystal interface (Greenham et al., 1996). Furthermore, the interface band bending creates the electron depletion region (W) at the ZnO particle surfaces and the conversion of the radiative V_0^+ centers to the nonradiative V_0^{++} state. As a result, blue emission becomes dominant. This mechanism is reversible and when the bias becomes zero, the green radiative recombination channel from the V_0^+ related states as well as PDPV emission should become dominant again in agreement with our experimental data. Note that the band bending in our experiment does not affect red emission, which is attributed to the deeper levels. A depletion region width (W) on the surface of ZnO particles depends on the surface state density and the charge carrier density in particles as it can be seen from equation 3 :

$$W=(2\varepsilon_{Zn0}V_{bi}/eN_d)^{1/2} \quad (3)$$

where ε_{Zn0}- is dielectric constatnt of ZnO, V_{bi} – potential barrier, e-electron charge, N_d – donor density. The size of particles and their charge density can control the luminescence spectrum. It is noteworthy that the CL spectrum of the PDPV–ZnO:Mg film contains peaks at ultraviolet-blue, blue-green, and red regions. This multicolor CL and the ability to tune the intensity of the bands by an electric field makes this polymer-nanoparticles composite promising for the creation of flexible tunable light emitters.

3.4 Optical tuning the luminescence of nanocrystals

The possibility of optical control of luminescence from nanocrystals was investigated by (Shih et al., 2011; Kurbanov et al., 2008a, 2008b). The visible light illumination effect on near-band-edge emission intensity from ZnO nanocrystals excited by UV He-Cd laser radiation (325 nm) was reported by (Kurbanov et al., 2008a). A cw Ar^+-laser irradiation (488 nm) in addition to the UV excitation can effectively (up to 75%) reduce the exciton emission from ZnO. This reduction in integrated intensity ($\Delta I/I$)(quenching) of the near-band-edge emission is reversible and has a pronounced dependence on temperature and ratio of Ar^+ and He-Cd laser power densities. The mechanism of the observed quenching effect was proposed to be similar the mechanism for the electric field tuned emission from ZnO nanocrystals in PDPV (Section 3.3). It implies an appearance of the additional recombination channel under a visible light illumination due to the recharging of oxygen-vacancy states in the surface depletion zone. The ZnO nanocrystals investigated in this work have the regular cone form and the size of 100–500 nm (Kurbanov et al., 2007a; Wang et al., 2005). PL studies were carried out on a SPEX spectrometer equipped with a 0.75 m grating monochromator using a 50 mW cw He-Cd laser operating at the wavelength of 325 nm as the excitation source. PL spectra were measured in the backscattering configuration and the registration of the PL signal was carried out by using a conventional lock-in technique with a mechanical chopper. A 12 mW cw Ar^+-laser operating at the wavelength of 488 nm (2.54 eV) was used as an additional illumination source. Both the laser beams were focused on the sample by employing quartz lenses. The beam spot size after the lens was estimated to be about 100 μm in diameter and the Ar^+-laser beam's spot covered the He-Cd-laser's spot. In order to vary the excitation intensity (power density), the spot size was kept constant while the input power was attenuated by the neutral filters. The corresponding maximum intensities of laser beams at 325 and 488 nm were estimated to be about 500 and 120 W/cm^2, respectively. The samples were mounted on the cold finger of a closed-cycle helium cryostat and the sample temperature was controlled in the range from 10 K up to room temperature. Figures 3.11 (a) and (b) display the RT PL spectra collected from ZnO nanocrystals under single (He-Cd laser) (black) and double (He-Cd and Ar^+-lasers) (red) illuminations at different excitation power densities of He-Cd laser. The quenching effect depends strongly on the power-density ratio of the employed lasers (I_{488}/I_{325})-with increasing the (I_{488}/I_{325}) ratio the magnitude of the quenching increases. A decrease in power density of the He-Cd laser by 2 orders of magnitude, at the constant Ar^+-laser intensity of 120 W/cm^2, results in an increase in the integrated intensity quenching ($\Delta I/I$) of the UV emission from 0.07 (7%) to 0.14 (14%). The observed quenching effect is reversible; the PL restores the initial intensity and form instantly after the turning off the Ar^+-laser illumination regardless of excitation power density.

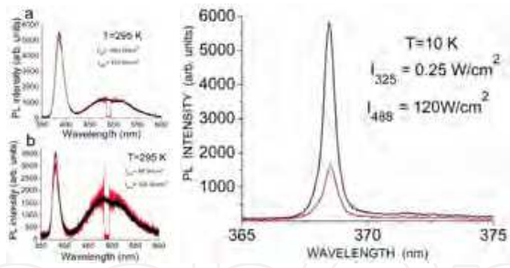

Fig. 3.11. (Left) RT PL spectra collected from CSD ZnO nanocrystals under single (He-Cd laser) (black) and double (He-Cd and Ar^+-lasers) (red) laser illuminations at different excitation power densities of He-Cd laser: (a) I_{325}~500 W/cm² and I_{488} ~120 W/cm² and (b) I_{325}~50 W/cm² and I_{488}~120 W/cm². (To protect the photomultiplier tube from the scattered Ar^+-laser radiation around 488 nm the spectrometer's slit was shut down). (Right) PL spectra collected from CSD ZnO nanocrystals under single (He-Cd laser) (black) and double (He-Cd and Ar^+-lasers) (red) laser illuminations at different excitation power densities of He-Cd laser at 10 K: I_{325}~0.25 W/cm² and I_{488}~120 W/cm².

The UV emission quenching effect was found to depend strongly on temperature and the laser power density. With the decrease in temperature to 10 K the magnitude of the quenching increases and under the He-Cd laser power density of 50 W/cm², it reaches to 0.38 (38%). The reducing of the He-Cd laser power density by 2 orders of magnitude at the fixed Ar^+-laser power density increases the quenching value up to 0.55 (55%) (Kurbanov et al., 2008a). The highest effect achieved in these experiments was ~75%. It was obtained at 10 K when the power-density ratio of the Ar^+ and He-Cd lasers was 500 (Fig. 3.11, right panel). The reversible behavior of the quenching effect remains also at low temperatures. However the time required reestablishing the initial PL intensity increases with a decrease in temperature. At 10 K the recovery time takes several minutes. Moreover the recovery time was found to depend on an illumination time by Ar^+-laser. The long term illumination results in prolongation of the recovery time of the PL intensity. The restoration of the PL initial intensity could be significantly accelerated by using a short-term increasing of temperature.

3.4.1 Electro-optical processes in nanocrystals under double excitation

The additional Ar^+-laser illumination of ZnO nanocrystals creates a new partway for excited charge-carrier recombination, which results in quenching of the near-band-edge emission intensity. Obviously, the energy of Ar^+-laser radiation (2.54 eV) is not enough to create new defects in ZnO lattice. However such low-energy photons can effect on charge states of the existing defects. As was identified in previous studies, the major defect related PL band at around 500 nm is originated from oxygen-vacancy center and the quenching effect also was more pronounced in samples with higher relative intensity of this band. Oxygen vacancies in ZnO can occur in three different charge states: the $V_0°$ state which has captured two electrons and is neutral relative to the lattice, the singly ionized V_0^+ state with one electron, and the V_0^{++} state which has no electrons and is doubly positively charged with respect to the lattice. Only the V_0^+ state is radiative and paramagnetic and consequently observable by EPR measurements. It is well known that the ZnO particle surface layer contains an electron depletion region created due to the surface states. The existence of such region results in the

band bending at the surface. In the fraction of the depletion region where the Fermi level passes below the V_0^+ /V_0^{++} energy level, all oxygen vacancies will be in the diamagnetic V_0^{++} state while oxygen vacancies in V_0^+ state will exist in the particle core. The first principle studies have shown (Lany & Zunger, (2005); Kohan et al., 2000; Van de Walle, 2001; Zhang et al., 2001) that the oxygen vacancy is a "negative-U" center, i.e., V_0^+ state is deeper (farther from the conduction band) than either V_0^{++} or $V_0°$ for any Fermi-level position. As already mentioned the intensity of the green luminescence in ZnO correlates very well with the paramagnetic single-ionized oxygen-vacancy density (Vanheusden et al., 1996a, 1996b). V_0^+ is found to be photosensitive for photons with an energy of >2 eV and this effect was explained by converting some of the V_0^{++} centers to the paramagnetic V_0^+ state. Considering these results and fact that the photon energy of Ar^+-laser radiation is 2.54 eV, the observed quenching effect of the near-band-edge emission from ZnO nanocrystals is well interpreted in terms of recharging of the oxygen-vacancy centers. Since V_0^{++} centers can be easily formed in the depletion region, consequently their number depends on the depletion region width (see Eq.3, Sec. 3.3.2). As can be seen, the width of the depletion region is inversely proportional to the square root of the free-carrier concentration in the nanocrystal and proportional to the potential at the surface. It is well known that in the case of high excitation, the surface potential depends on excitation intensity (Studenikin et al., 1998a). At high intensities the width of the depletion region is smaller than at low intensities. On the other hand an increase in temperature leads to additional narrowing of the depletion region due to the increase in the free carrier concentration. The simultaneous action of these factors (i.e., the increase in excitation intensity and temperature) results in the strong decrease in the depletion region width, consequently, the concentration of V_0^{++} centers. These speculations are in the good agreement with a strong increase in the quenching effect with a decrease in excitation power density and temperature. The temperature lowering from 295 to 10 K and a decrease in excitation intensity in 3 orders of magnitude (from 500 to 0.5 W/cm^2) resulted in a large enhancement of the quenching effect (from 7% up to 53%) at the fixed Ar^+-laser power density of 120 W/cm^2. Even though the Ar^+-laser illumination quenches well the UV emission, its impact on the visible emission intensity is observed very week. Although at room temperature under the double illumination the visible emission intensity slightly increases, at low temperatures it is rather unremarkable. This circumstance may be originated from different excitation efficiencies of the UV and visible emissions depending on temperature and excitation power density. One can see a decrease in temperature results in an increase in ratio of intensity of the UV emission to that of the visible emission. It increases from 2.25 to 66.5 with the decrease in temperature from 295 to 10 K at low excitation power density. Such behavior indicates that at low temperatures the visible emission is excited with relatively low efficiency than UV emission and the effect of Ar^+-laser irradiation on the visible PL, probably, also decreases. On the other hand, Ar^+-laser illumination could induce mostly the nonradiative states. It is known that there exists another type of single-ionized oxygen-vacancy-related center: V_0^+ complex, (Vanheusden et al., 1997) which can be formed in the presence of nearby interstitial oxygen (Frenkel pair) (Hoffmann & Hahn, 1974). This center unlike the isolated V_0^+ is not a green luminescent site, even though it shows a somewhat similar nature. Moreover the V_0^+ complex may act as a quenching center for radiative recombination in ZnO. The CSD technique used to grow ZnO nanocrystals provides the oxygen rich samples (Kurbanov et al., 2007a). This circumstance allows us to infer that in the ZnO nanocrystals

prepared in the oxygen rich conditions, some of V_0^{++} centers under Ar^+-laser illumination creates V_0^+ -complex which does not take part in green emission but acts as nonradiative, quenching center for UV PL. The reversible behavior of the quenching effect and dependence of the recovery time on temperature and exposure time by the visible light confirm the proposed recharging model of the oxygen-vacancy-related centers in the ZnO nanocrystal depletion region. As was reported (Vanheusden 1996a), the EPR signal from V_0^+ decays when illumination was interrupted and at 294 K this decay is instantaneous, but at 150 K it requires several minutes. In our experiments the recovery process of the UV emission intensity could be also accelerated by a short-term rising of temperature. These observations indicate that there is some energetic barrier, escaping of which the system can return into the initial state. The existence of energetic barrier for decay of photogenerated V_0^+ into the other charge states was predicted by Walle (Van de Walle, 2001) based on the first principles investigation. For a further understanding of the mechanism of the observed UV PL band quenching, we investigated the quenching effect dependence on the excitation power density in details. The integrated PL intensity versus the excitation power density under (a) the single (He-Cd laser) and (b) the double (He-Cd-and Ar^+-lasers) illuminations as well as (c) the quenching ($\Delta I/I$) of the UV emission at 10 K are plotted in Fig. 3.12. The both PL intensity dependences display a tendency to saturation at high excitation level. The luminescence intensity I versus excitation power density can be expressed as

$$I = \eta I_0^{\alpha} \tag{4}$$

In this relation I_0 is the power density of the excitation laser radiation, η is the constant of proportionality (some authors define it as an emission efficiency), and the exponent a represents the radiative recombination mechanism. For excitonic recombination, $1<a<2$, for band-gap emission, i.e., electron-hole bimolecular recombination, $a\sim 2$, and a is less than 1 when an impurity is involved in the transitions, as well as for donor-acceptor transitions (Bergman et al., 2004; Jin et al., 1997). Using Eq. (4) to fit the data of the single and double laser illuminations we found a ~0.61 and a~0.7, respectively. The obtained values of the exponent a are less 1 and they could be interpreted as evidence that the UV emission originates from native donor-acceptor transitions or impurities. However all results undoubtedly indicate that UV PL has exciton nature. As is well known, a saturation effect of the excitonic emission under high-power excitation is not rarely observed phenomenon (Bergman et al., 2004; Jin et al., 1997). The saturation of the excitonic emission from GaN powder excited in ambient air at RT was ascribed to a thermally activated nonradiative process due to laser heating of particles (Bergman et al., 2004). A slow increase and saturation of the PL intensity of free excitons in a GaInAsSb/GaAlAsSb single-quantum-well structure under higher excitation intensity observed at 10 K was attributed to the exciton screening effect (Jin et al., 1997). It seems in our experiment that both suggested saturation mechanisms are present.

The visible light illumination increases the exponent α from 0.61 to 0.70 by of approximately 15%. This growth undoubtedly is not result of a decrease in the laser heating. It originates rather from a decrease in exciton relative population due to opening an additional channel of recombination. Although this channel is basically nonradiative, the decrease in exciton relative population can reduce the exciton screening effect and provide a faster increase in the PL intensity with excitation power than that in the case of the single He-Cd laser

illumination. It may be expected that use of the observed quenching effect allows effectively modulate the UV emission from ZnO and an employment of high power lasers with wavelength in the 450–550 nm region could provide it.

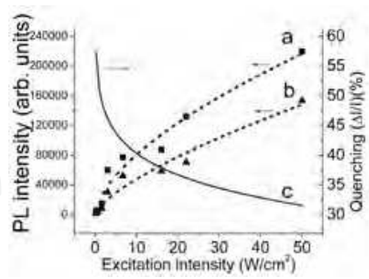

Fig. 3.12. Integrated exciton PL intensity (a) without and (b) under Ar^+-laser illumination as well as (c) the quenching of the PL intensity as a function of He-Cd laser excitation power density at 10 K. The dash lines are the fit to a power law (see the text) (Kurbanov et al., 2008a).

3.4.2 The optical modulation of UV PL from ZnO nanocrystals

The optical modulation of ultraviolet (UV) photoluminescence from ZnO nanocrystals excited by He–Cd laser (325 nm) with visible Ar^+ laser radiation (488 nm) was reported by (Kurbanov et al., 2008b). The effective reversible quenching of the UV luminescence intensity was achieved. The quenching efficiency was found to depend on temperature, the ratio of He–Cd and Ar^+ laser intensities, and the frequency of modulation. The observed quenching effect was used to modulate UV emission by chopped visible Ar^+ laser radiation. A sufficiently large modulation depth was obtained.

Figure 3.13 (solid line) shows the PL spectrum of ZnO nanocrystals obtained at 10K under radiations with the He–Cd laser. The spectrum displays a dominant near-band-edge emission peak at 368.6 nm and two weak emission bands at 373.6 and 382.8 nm as well as a weak visible emission band. The peak around 368 nm is related to the PL emission of a donor bound exciton (Kang et al., 2005; Look, 2001; Özgür et al. 2005). The bands at 373.6 and 382.8 nm, as indicated by arrows in Fig. 3.13, might be attributed to donor–acceptor pair recombination (Tomzig & Helbig, 1976) or exciton phonon replicas (Reynolds & Collins, 1969) or two photon transitions (Studenikin et al., 2000). An additional radiation using the Ar^+ laser leads to the strong quenching of the UV emission up to approximately 55% with some changes in deep-level PL [Fig. 3.13 (dashed line)].

The Ar^+-laser-radiation-induced quenching effect was used to modulate the intensity of the UV emission from ZnO nanocrystals. For this objective, the ZnO nanocrystals at 10K were simultaneously excited using an unmodulated cw He–Cd laser beam and a chopped Ar^+ laser beam. The power densities of the UV and visible lasers were 0.5 and 120W/cm^2, respectively. The UV peak intensity variations at 368.6 nm were observed using a SPEX monochromator and a photomultiplier tube on a Tektronix oscilloscope. The intensity variations of the exciton emissions at different modulation frequencies of the Ar^+ laser are presented in Fig. 3.13 (right panel). The curve (a) (Fig. 3.13. (Right)) represents the dc PL signal from the ZnO nanocrystals obtained under the single cw He–Cd laser excitation. The curves (b), (c), and (d) are PL signals modulated by Ar^+ laser radiation in various frequency

regions: low (20 Hz), middle (200 Hz), and high (400 Hz), respectively. With increasing Ar^+ laser beam modulation frequency, both the amplitude of the PL signal and its mean level decrease. The curve (e) represents the dc PL signal obtained when nanocrystals were illuminated with an unmodulated cw Ar^+ laser beam. It was the lowest level that was achieved under Ar^+ laser radiation. The decrease in the modulation depth of the PL intensity with increasing frequency at low temperature is caused by the long recovery time of the quenching effect. As can be seen from Fig. 3.13, the complete modulation {i.e., the change in the PL intensity from the initial level to the lowest level induced by cw Ar laser radiation [curve (e)]} was observed at low (10– 20 Hz) modulation frequencies. It seems reasonable to expect that the complete modulation of the UV emission at RT could be obtained at higher frequencies. However, a high-power Ar^+ laser or a pulse laser operating in the 480 – 500 nm range should be employed owing to the small magnitude of the quenching effect at 300 K.

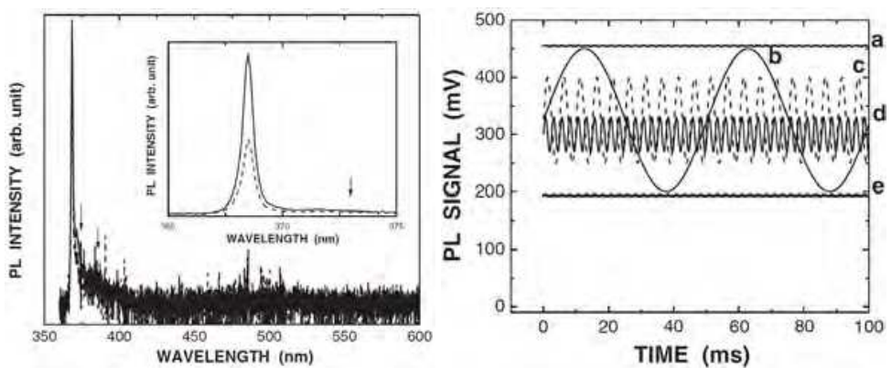

Fig. 3.13. (Left) PL spectra of ZnO nanocrystals obtained at 10K under He–Cd laser excitation (soid line) and combined He–Cd and Ar^+ laser radiations (dashed line). (The intensities of the He–Cd and Ar^+ lasers are approximately 0.50 and 120 W/cm^2, respectively.) The inset shows the PL spectra in the wavelength range between 365 and 375 nm. (Right) Schematics of PL signals from ZnO nanocrystals at 10K observed using oscilloscope. The curve (a) indicates the dc PL signal from ZnO nanocrystals under cw He–Cd laser excitation and the curves (b), (c), and (d) represent the PL signals modulated by Ar^+ laser radiation under cw He–Cd laser excitation at approximately 20, 200, and 450 Hz, respectively. The curve (e) represents the dc PL signal under both cw He–Cd and Ar^+ laser radiations.

4. Conclusion

In this chapter recent progress in multicolor luminescence from semiconductor nanocrystal composites tunable in an electric field have been highlighted. The effect of an external electric field on cathodoluminescence from semiconductor nanocrystals and nanocomposites with different radiative emission rates was described, giving special emphasis to ZnO nanocrystals in MgO and polymer matrix. The structural and optical properties ZnO nanocrystals and nanocomposites, including the core/shell nanocrystals were investigated. An ability to control the relative intensity of the near-band-gap emission (UV, violet-blue) and the deep-level luminescence (green, red) from ZnO nanocrystals and polymer composites by an electron-hole pumping and an electric field was demonstrated. It allows to adjust the luminescence of the composite in a broad visible wavelength range. The effect of an external electric field on cathodoluminescence

from the nanocrystal/polymer structure was studied, giving special emphasis to the doped ZnO nanocrystals in Poly(4,4′- diphenylene diphenylvinylene) (PDPV) matrix and PBET/ITO structures. Cathodoluminescence of the polythiophene derivative structure was investigated under various electron beam current excitations. UV and blue bands in the spectrum of the polymer structure at the high electron beam current density are observed. The intensities of these bands increase as an electron beam current density increases while the green–orange luminescence is saturated. The induced electron beam field in the PBET/ITO suggests inhibiting the green luminescence by dissociation of the excitons, thereby enhancing the direct interband radiative transition with UV emission. The room temperature electron beam irradiation with a large fluence at a high current density results in the broad blue luminescence that may be attributed to the electron/structural changes in the polythiophene derivate film under an induced electric field. These effects could be used to obtain white light luminescence from the polythiophene derivative composites. Electric field-induced color switching of cathodoluminescence from ZnO:Mg nanocrystals/PDPV composite from blue-green to red is considered. The assumed mechanism of electric field-tunable cathodoluminescence implies the presence of radiative recombination channels, which are sensitive to the electric field through the band bending at the crystal surface. Optical control luminescence through the impact of visible Ar^+-laser illumination (488 nm) on the UV emission from ZnO nanocrystals excited by He-Cd laser (325 nm) at various excitation intensities and temperatures has been investigated. It was found that a visible light illumination simultaneously with UV excitation results in a decrease in the near-band-edge emission intensity. The experiments on a reversible quenching of the UV near-band-edge emission under Ar^+-laser illumination confirm an appearance of the recombination channel after oxygen-vacancy charging in the ZnO surface depletion zone. The quenching effect of the UV emission observed in ZnO samples is suggested to be due to the recharging of oxygen-vacancy states under a visible light irradiation. The strong quenching of UV luminescence from ZnO nanocrystals under Ar^+-laser illumination (488 nm) and an opportunity to modulate the UV PL intensity by visible light irradiation was demonstrated. The quenching effect depends on the intensity ratio of the visible and UV lasers, temperature, and the relative intensity of the green luminescence band. The highest quenching effect (75%) was achieved at I_{488}/I_{325}~500 at 10 K. It was shown that the UV near-band-edge emission is modulated at frequencies of hundreds of hertz. It is reasonable to expect that the complete modulation of the UV emission at RT could be obtained at higher frequencies when using a high-power Ar^+ laser or a pulse laser operating in the 480 – 500 nm range. In this context the quenching effect may find application in ZnO based optoelectronic devices and optical communication systems.

5. Acknowledgment

This work was supported by a National Research Foundation of Korea (NRF) grant funded by the Ministry of Education, Science and Technology (MEST) No. 2011-0000016 as well as by the Leading Foreign Research Institute Recruitment Program through NRF funded by MEST No. 2010-00218, and a Russian Ministry of Science and Education grant No. 02.740.11.5215. Author is grateful to all colleagues who took part in joint work, especially A.N. Baranov, O.O. Kapitanova, S.S. Kurbanov, A.N. Aleshin, I. A. Khotina, and T.W. Kang.

6. References

Ahn S.H., Czae M.Z., Kim E.R., Lee H., Han S.H., Noh J. & Hara M. (2001). Synthesis and Characterization of Soluble Polythiophene Derivatives Containing Electron-Transporting Moiety. Macromolecules, 34, pp. 2522-2527.

Ahn T., Lee H. & Han S.-H. Effect of annealing of polythiophene derivative for polymer light-emitting diodes. Appl. Phys. Lett. 80, pp. 392-394

Aigouy L., Holden T., Pollak F. H., Ledentsov N. N., Ustinov W. M., Kopev P. S. & Bimberg D. (1997). Contactless electroreflectance study of a vertically coupled quantum dot-based InAs/GaAs laser structure. Appl. Phys. Lett. 70, pp. 3329-3331.

Andersen K.E.; Fong C.Y. & Pickett W.E. (2002). Quantum confinement in CdSe nanocrystallites. J.Non. Cryst. Solids 99, pp.1105-1110.

Artbauer J. (1996). Electric strength of polymers. J. Phys. D 29, pp. 446-456.

Bagnall D.M., Chen Y.F., Zhu Z., Yao T., Koyama S., Shen M.Y & Goto T. (1997). Optically pumped lasing of ZnO at room temperature. Appl. Phys. Lett. 70, pp. 2230-2232.

Baranov A N, Chang C H, Shlyakhtin O A, Panin G N, Kang T W & Oh Y J (2004). In situ study of the ZnO–NaCl system during the growth of ZnO nanorods. Nanotechnology 15, pp. 1613-1619.

Baranov A N, Solozhenko V L, Chateau C, Bocquillon G, Petitet J P, Panin G N, Kang T W, Shpanchenko R V, Antipov E V & Oh Y J (2005a). Cubic MgxZn1−xO wide band gap solid solutions synthesized at high pressures.: J. Phys.:Condens. Matter 17, pp. 3377–3384

Baranov A N, Panin G N, Kang Tae Wong & Oh Young-Jei (2005b). Growth of ZnO nanorods from a salt mixture. Nanotechnology 16, pp. 1918–1923

Baranov A. N.; Panin G. N.; Yoshimura Masahiro & Oh Young-Jei (2006). Growth and magnetic properties of Mn and MnSn doped ZnO nanorods. J. Electroceram., 17, pp. 847-852.

Baranov A. N., Kapitanova O. O., Panin G. N. & Kang T. V. (2008). ZnO/MgO Nanocomposites Generated from Alcoholic Solutions. Russ. J. of Inorg. Chem., 53 (9), pp. 1366-1370.

Baranov A. N.; Kurakevych O. O.; Tafeenko V. A.; Sokolov P. S.; Panin G. N. & Solozhenkopp V. L. (2010). High-pressure synthesis and luminescent properties of cubic ZnO/MgO nanocomposites. J. Appl. Phys. 107, pp. 073519-1-073519-5.

Bergman L., Chen X. B., Morrison J. L., Huso J. & Purdy A. P. (2004). Photoluminescence dynamics in ensembles of wide-band-gap nanocrystallites and powders. J. Appl. Phys. 96, pp. 675-682.

Borgohain K. & Mahamuni S. (1998). Luminescence behaviour of chemically grown ZnO quantum dots. Technol. 13, pp. 1154-1157.

Bojarski P. (2002). Concentration quenching and depolarization of rhodamine 6G in the presence of fluorescent dimers in polyvinyl alcohol films. Chem. Phys. Lett. 278, pp. 225-232.

Bredas J.-L., Cornil J. & Heeger A.J. (1996). The exciton binding energy in luminescent conjugated polymers. Adv. Mater. 8, pp. 447-452.

Bredas J. L., Logdlund M. & Salaneck W. R. (1999). Electroluminescence in conjugated polymers Nature, 397, pp. 121-128.

Bylander E. G. (1978). Surface effects on the low-energy cathodoluminescence of zinc oxide. J. Appl. Phys. 49, pp. 1188-1195.

Burroughes J.M., Burroughes J. H., Bradley D. D. C., Brown A. R., Marks R. N., Mackay K., Friend R. H, Burns P. L. & Holmes A. B. (1990). Nature (London) 347, pp. 539-541.

Brus L.E. (1984). Electron–electron and electron-hole interactions in small semiconductor crystallites: The size dependence of the lowest excited electronic state. J. Chem. Phys. 80. pp. 4403-4409.

Brus L.E. (1986). Electronic wave functions in semiconductor clusters: experiment and theory. J. Phys. Chem. 90, p. 2555-2560.

Cacialli F., Friend R. H., Haylett N., Daik R., Feast W. J., Dos Santos D. A. & Bredas J. L., (1997). Efficient green light emitting diodes from a phenylated derivative of poly(p-Phenylene-Vinylene). Synth. Metals, 84, pp. 643-644.

Cao B. Q., Lorenz M., Rahm A., von Wenckstern H., Czekalla C., Lenzner J., Benndorf G. & Grundmann M. (2007). Phosphorus acceptor doped ZnO nanowires prepared by pulsed-laser deposition. Nanotechnology 18, pp. 455707.

Cao H., Zhao Y. G., Ho S. T., Seelig E. W., Wang Q. H. & Chang R. P. H. (1999). Random Laser Action in Semiconductor Powder. Phys. Rev. Lett. 82, pp. 2278-2281.

Chayet H; Pogreb R. & Davidov D. (1997). Transient UV electroluminescence from poly(p-phenylenevinylene) conjugated polymer induced by strong voltage pulses. Phys. Rev. B 56 (20), pp. 12702-12705.

Chen I. J.; Chen T. T.; Chen Y. F. & T. Y. Lin (1996). Nonradiative traps in InGaN/GaN multiple quantum wells revealed by two wavelength excitation. Appl. Phys. Lett. 89, 142113-142115.

Chen W., Wang Z. G., Lin Z. J. & Lin L. (1997). Absorption and luminescence of the surface states in ZnS nanoparticles J. Appl. Phys. 82, p. 3111-3115.

Cheng W.; Wu P.; Zou X. & Xiao T. (2006). Study on synthesis and blue emission mechanism of ZnO tetrapodlike nanostructures. J. Appl. Phys. 100, pp. 054311(4).

Combescot M, Combestcot R & Roulet B (2001). The exciton dead layer revisited. Eur. Phys. J. B 23 139-151.

Dingle R. (1969). Luminescent Transitions Associated With Divalent Copper Impurities and the Green Emission from Semiconducting Zinc Oxide. Phys. Rev. Lett. 23, pp. 579-581.

Djuris˘ic A. B., Leung Y. H., Tam K. H., Ding L., Ge W. K., Chen H. Y. & Gwo S. (2006). Green, yellow, and orange defect emission from ZnO nanostructures: Influence of excitation wavelength. Appl. Phys. Lett. 88, pp. 103107(3).

Du X.W., Fu Y.S., Sun J., Han X. & Liu J. (2006). Complete UV emission of ZnO nanoparticles in a PMMA matrix. Semicond. Sci. Technol. 21, pp. 1202-1206.

Efros A.L. & Rosen M. (2000). The electronic structure of semiconductor nanocrystals. Annu. Rev. Mater. Res, 30 pp. 475-521.

Egelhaaf H. J. & Oelkrug D. (1996). Luminescence and nonradiative deactivation of excited states involving oxygen defect centers in polycrystalline ZnO. J. Cryst. Growth 161, pp. 190-194.

Erhart P., Albe K. and Klein A. (2006).First-principles study of intrinsic point defects in ZnO: Role of band structure, volume relaxation, and finite-size effects. Phys. Rev. B 73, pp. 205203(9).

Ethiraja A.S., Hebalkara N., Kharrazia Sh., Urban J., Sainkar S.R., Kulkarn S.K. (2005). Photoluminescent core-shell particles of organic dye in silica. J. Lumin. 114, pp. 15-23.

Falcony C., Ortiz A., Garcia M. & Helman J. S. (1988).Photoluminescence characteristics of undoped and terbium chloride doped zinc oxide films deposited by spray pyrolysis.J. Appl. Phys. 63, pp. 2378-2388.

Fallert J., Hauschild R., Stelzl F., Urban A., Wissinger M., Zhou H., Klingshirn C. & Kalt H., (2007). Surface-state related luminescence in ZnO nanocrystals. J. Appl. Phys. 101, pp. 073506(4).

Feast W. J., Millichamp I. S., Friend R. H., Horton M. E., Phillips D., Rughooputh S. D. D. V. & Rumbles G. (1985). Optical absorption and luminescence in poly(4,4′-diphenylenediphenylvinylene). Synth. Metals 10, pp. 181-191.

Fonoberov V. A., Alim K. A., Balandin A. A., Xiu F. & Liu J. (2006). Photoluminescence investigation of the carrier recombination processes in ZnO quantum dots and nanocrystals. Phys. Rev. B 73, pp. 165317(9).

Fonoberov V A & Balandin A. A. (2004). Radiative lifetime of excitons in ZnO nanocrystals: The dead-layer effect. Phys. Rev. B 70, pp. 195410(5).

Friend R. H., Gymer R. W., Holmes A. B., Burroughes J. H., Marks R. N., Taliani C., Bradley D. D. C., Dos Santos D. A., Bredas J. L., Logdlund M. & Salaneck W. R. (1999). Electroluminescence in conjugated polymers. Nature, 397, pp. 121-128.

Fu D. J., Panin G. N. & Kang T. W. (2003). GaN Pyramids Prepared by Photo-Assisted Chemical Etching. Journal of the Korean Physical Society, Vol. 42, pp. S611-S613.

Fu Dejun; Park Young Shin; Panin Gennady N. & Kang Tae Won (2005). Formation of Hexagonal GaN Pyramids by Photo Assisted Electroless Chemical Etching. Jap. Journal of Applied Phys, Vol.44, No.11, pp. L342-L344.

Gaspar C., Costa F. & Monteiro T. (2001). Optical characterization of ZnO. J. Mater. Sci.: Mater. Electron. 12, pp. 269-271.

Gill B. & Kavokin A. V. (2002). Giant exciton-light coupling in ZnO quantum dots. Appl. Phys. Lett. 81, pp. 748-750.

Greenham N. C., Peng Xiaogang & Alivisatos A. P. (1996). Charge separation and transport in conjugated-polymer/semiconductor-nanocrystal composites studied by photoluminescence quenching and photoconductivity. Phys. Rev. B 54, pp. 17628-17637.

Hagn M., Zrenner A., Böhm G. & Weimann G. (1995). Electric-field-induced exciton transport in coupled quantum well structures, Appl. Phys. Lett. 67 (2), pp. 232-234.

Harada Y. & Hashimoto S. (2003). Enhancement of band-edge photoluminescence of bulk ZnO single crystals coated with alkali halide. Phys. Rev. B 68, pp. 045421(4).

He H. P., Tang H. P., Z. Z. Ye, Zhu L. P., Zhao B. H., Wang L. & Li X. H. (2007). Temperature-dependent photoluminescence of quasialigned Al-doped ZnO nanorods. Appl. Phys. Lett. 90, pp. 023104(3).

Hirai T., Ohno N., Harada Y., Horii T., Sawada Y. & Itoh T. (2008). Spatially resolved cathodoluminescence spectra of excitons in a ZnO microparticle. Appl. Phys. Lett. 93, pp. 041113(3).

Hoffmann K. & Hahn D. (1974). Electron Spin Resonance of Lattice Defects in Zinc Oxide. Phys. Status Solidi A 24, pp. 637-648.

Hosaka N., Tachibana H., Shiga N., Matsumoto M., & Tokura Y. (1999). Photoinduced Phase Transformation in Polythiophene. Phys. Rev. 82 , pp. 1672-1675.

Hosono Eiji, Fujihara Shinobu, Kimura Toshio & Imai Hiroaki (2004). Non-Basic Solution Routes to Prepare ZnO Nanoparticles. J. Sol-Gel Sci. Technol. 29, pp. 71-79.

Hyberstsen M.S. (1994). Absorption and emission of light in nanoscale silicon structures. Phys. Rev. Lett. 72, p. 1514-1517.

Hua G., Zhang Y., Ye Ch., Wang M. & Zhang L. (2007).Controllable growth of ZnO nanoarrays in aqueous solution and their optical properties. Nanotechnology 18, pp. 145605

Hur T B, Hwang Y H & Kim H. K. (2005). Quantum confinement in Volmer–Weber-type self-assembled ZnO nanocrystals. Appl. Phys. Lett. 86, pp. 193113(3).

Innocenzi P., Kozuka H. & Yoko T. (1996). Dimer-to-monomer transformation of rhodamine 6G in sol—gel silica films. J. Non-Crystal. Sol. 201, pp. 26-36.

Yamamoto A., Kido T., Goto T., Chen Y., Yao T. & Kasuya A. (1999). Dynamics of photoexcited carriers in ZnO epitaxial thin films. Appl. Phys. Lett. 75, pp. 469-471.

Jeong S.H., Kim B.S. & Lee B.T. (2003). Photoluminescence dependence of ZnO films grown on Si(100) by radio-frequency magnetron sputtering on the growth ambient. Appl. Phys. Lett. 82, pp. 2625-2627.

Jin Sh., Zheng Y. & Li A. (1997). Characterization of photoluminescence intensity and efficiency of free excitons in semiconductor quantum well structures. J. Appl. Phys. 82, pp. 3870-3873.

Johnson P.D. (1954). Some Optical Properties of MgO in the Vacuum Ultraviolet. Phys. Rev. 94, pp. 845-846.

Yu P., Tang Z.K., Wong G.K.L., Kawasaki M., Ohtomo A., Koinuma H. & Segawa Y. (1997). Ultraviolet spontaneous and stimulated emissions from ZnO microcrystallite thin films at room temperature. Solid State Commun. 103, pp. 459-463.

Kang T. W.; Yuldashev Sh. & Panin G. N. (2006). Electrical and optical properties of ZnO thin films and nanostructures. Chapter 4, In Handbook of Semiconductor Nanostructures and Nanodevices, edited by A. A. Balandin and K. L. Wang, American Scientific, Los Angeles.

Kasai P. H. (1963). Electron Spin Resonance Studies of Donors and Acceptors in ZnO. Phys. Rev. 130, pp. 989-995.

Klik M. A. J.; Gregorkiewicz T.; Yassievich I. N.; Ivanov V. Yu. & Godlewski M. (2005). Terahertz modulation of the blue photoluminescence in ZnSe. Phys. Rev. B 72, pp. 125205(5).

Kohan A. F., Ceder G., Morgan D. & Van de Walle Chris G. (2000). First-principles study of native point defects in ZnO. Phys. Rev. B 61, pp. 15019-15027.

Kroger E. A. & Vink H. J. (1954). The Origin of the Fluorescence in Self-Activated ZnS, CdS, and ZnO. J. Chem. Phys. 22, pp. 250-252.

Koshihara S., Tokura Y., Takeda K. & Koda T. (1992). Reversible photoinduced phase transitions in single crystals of polydiacetylenes. Phys. Rev. Lett. 68, pp. 1148-1151.

Kumar B., Gonga H., Vicknesh S., Chua S.J. & Tripathy S. (2006). Luminescence properties of ZnO layers grown on Si-on-insulator substrates. Appl. Phys. Lett. 89, pp. 141901(3).

Kurbanov S., Panin G., Kim T. W. & T. W. Kang (2007a). Thermo- and Photo-annealing of ZnO Nanocrystals. Jpn. J. Appl. Phys., Part 1 46, pp. 4172-4174

Kurbanov S.S., Panin G.N., Kim T.W. & Kang T.W. (2007b). Luminescence of ZnO nanocrystals capped with an organic dye. Optics Communications 276, pp. 127–130.

Kurbanov S.S., Panin G. N., Park Y. S., Kang T. W. & Kim T. W. (2007c). Photo- and Cathodoluminescence Studies of ZnO-Filled Opal Nanocomposites. Journal of the Korean Physical Society, Vol. 50, No. 3, pp. 617-621.

Kurbanov S. S., Panin G. N., Kim T. W. & Kang T. W. (2008a). Impact of visible light illumination on ultraviolet emission from ZnO nanocrystals. Phys. Rev. B 78, pp. 045311-1-045311-6

Kurbanov Saidislam, Panin Gennady, Kang Tae Won & Kim Tae Whan (2008b). Modulation of Excitonic Emission from ZnO Nanocrystals by Visible Light Illumination. Jap. J. Appl. Phys. Vol. 47, No. 5, pp. 3760–3762.

Kurbanov S.S.; Panin G.N.; Kim T.W. & Kang T.W. (2008c). ZnO filled opal arrays: Photo- and cathodoluminescence studies. Solid State Communications, 145 (11-12), pp. 577-581.

Kurbanov S.; Panin G. & Kang T.M. (2009a). Spatially resolved investigations of the emission around 3.31 eV (A-line) from ZnO nanocrystals. Appl. Phys. Lett. 95, pp. 211902-1- 211902-3.

Kurbanov S.; Panin G.N.; Kim T.W. & Kang T.W. (2009b). Strong violet luminescence from ZnO nanocrystals grown by the low-temperature chemical solution deposition. Journal of Luminescence 129, pp. 1099–1104.

Lany S. & Zunger A. (2005). Anion vacancies as a source of persistent photoconductivity in II-VI and chalcopyrite semiconductors. Phys. Rev. B 72, pp. 035215(13).

Lee Sang Wuk; Cho Hak Dong; Panin Gennady & Kang Tae Won (2011). Vertical ZnO nanorod/Si contact light-emitting diode. Appl. Phys. Lett. 98, pp. 093110-1-093110-3

Leiter F. H.; Alves H. R.; Hofstaetter A.; Hofmann D. M. & Meyer B. K. (2001). The Oxygen Vacancy as the Origin of a Green Emission in Undoped ZnO. Phys. Status Solidi B 226, pp. R4-R5.

Levitsky I.A., Liang J. & Xu J.M. (2002). Highly ordered arrays of organic–inorganic nanophotonic composites. Appl. Phys. Lett. 81, pp. 1696-1698.

Liu B & Zeng H C (2004) Room Temperature Solution Synthesis of Monodispersed Single-Crystalline ZnO Nanorods and Derived Hierarchical Nanostructures. Langmuir 20, pp. 4196-4204.

Liu M., Kitai A. H. & Mascher P. (1992). Point defects and luminescence centres in zinc oxide and zinc oxide doped with manganese. J. Lumin. 54, pp. 35-42.

Look, C. (2001) Recent advances in ZnO materials and devices. Mater. Sci. Eng., B 80, pp. 383-387.

Look D. C., Reynolds D. C., Litton C. W., Jones R. L., Eason D. B. & Gantwell G. (2002). Characterization of homoepitaxial p-type ZnO grown by molecular beam epitaxy. Appl. Phys. Lett. 81, pp. 1830-1832.

Lyapina O. A., Baranov A. N., Panin G. N., Knotko A. V. & Kononenko O. V. (2008). Synthesis of ZnO Nanotetrapods. Inorganic Materials, Vol. 44, No. 8, pp. 845–851.

Makino T., Tamura K., Chai C.H., Segawa Y., Kawasaki M., Ohtomo A. & Koinuma H. (2002). Radiative recombination of electron–hole pairs spatially separated due to quantum-confined Stark and Franz–Keldish effects in ZnO/$Mg_{0.27}Zn_{0.73}O$ quantum wells. Appl. Phys. Lett. 81, pp. 2355-2357.

Mass J., Avella M., Jiménez J., Rodríguez A., Rodríguez T., Callahan M., Bliss D. & Wang B. (2008). Cathodoluminescence study of ZnO wafers cut from hydrothermal crystals. J. Cryst. Growth 310, pp. 1000-1005.

Massines F., Tiemblo P., Teyssedre G. & Laurent C. (1997),On the nature of the luminescence emitted by a polypropylene film after interaction with a cold plasma at low temperature. J. Appl. Phys. 81, pp. 937-943.

Matsumoto T., Kato H., Miyamoto K., Sano M. & Zhukov M. (2002). Correlation between grain size and optical properties in zinc oxide thin films. Appl. Phys. Lett. 81, pp. 1231-1233.

Meulenkamp E. A. (1998). Synthesis and Growth of ZnO Nanoparticles. J. Phys. Chem. B 102, pp. 5566-5572.

Meulenkamp E. A. (1998). Size Dependence of the Dissolution of ZnO Nanoparticles. J. Phys. Chem. B 102, pp. 7764-7769.

Meyer B. K., Alves H., Hofmann D. M., Kriegseis W., Forster D., Bertram F., Christen J., Hoffmann A., Straßburg M., Dworzak M., Haboeck U. & Rodina A. V. (2004). Bound exciton and donor–acceptor pair recombinations in ZnO. Phys. Status Solidi B 241, pp. 231-260.

Micheletto Ruggero Yoshimatsu Nobuki, Yokokawa Masatoshi, An Taekyung, Lee Haiwon & Okazaki Satoshi (2001). Optical study of a polymeric LED with a nano-sized electrode realized by a modified SNOM setup. Opt. Commun. 196, pp. 47-53.

Minne S.C., Manalis S.R. & Quate C.F. (1995). Parallel atomic force microscopy using cantilevers with integrated piezoresistive sensors and integrated piezoelectric actuators. Appl. Phys. Lett. 67, pp. 3918-3920.

Mitra A., Thareja R. K., Ganesan V., Gupa A., Sahoo P. K. & Kulkarni V. N., (2001). Synthesis and characterization of ZnO thin films for UV laser. Appl. Surf. Sci. 174, pp. 232-239.

Mordkovich V. Z., Hayashi H., Haemori M., Fukumura T. & Kawasaki M. (2003). Discovery and Optimization of New ZnO-Based Phosphors Using a Combinatorial Method. Adv. Funct. Mater. 13, pp. 519-524.

Motyka M., Sek G., Kudrawiec R., Misiewicz J., Li L. H. & Fiore A. (2006). On the modulation mechanisms in photoreflectance of an ensemble of self-assembled InAs/GaAs quantum dots. J. Appl. Phys. 100, pp. 073502(5).

Norberg N.S.& Gamelin D.R. (2005). Influence of Surface Modification on the Luminescence of Colloidal ZnO Nanocrystals. J. Phys. Chem. B 109, pp. 20810-20816.

Ohtomo A., Kawasaki M., Koida T., Masubuchi K., Koinuma H., Sakurai Y., Yoshida Y., Yasuda T. & Segawa Y. (1998). $Mg_xZn_{1-x}O$ as a II–VI widegap semiconductor alloy. Appl. Phys. Lett. 72, pp. 2466-2468.

Ohtomo A., Shiroki R., Ohkubo I., Koinuma H. & Kawasaki M. (1999). Thermal stability of supersaturated $Mg_xZn_{1-x}O$ alloy films and $Mg_xZn_{1-x}O$/ZnO heterointerfaces. Appl. Phys. Lett. 75, pp. 4088-4090.

Ohtomo A., Tamura K., Kawasaki M., Makino T., Segawa Y., Tang Z.K., Wong G.K.L., Matsumoto Y., & Koinuma H. (2000) Room-temperature stimulated emission of excitons in ZnO/(Mg,Zn)O Superlattices. Appl. Phys. Lett. 77, pp. 2204-2206.

Özgür Ü.; Alivov Ya. I.; Liu C.; Teke A.; Reshchikov M. A.; Doğan S.; Avrutin V.; Cho S.-J. & Morkoç H. (2005). A comprehensive review of ZnO materials and devices. J. Appl. Phys. 98, pp. 041301(103).

Panin G. N.; Kang T.W. & Jang M. S. (2003a). Spatially Resolved Study of Luminescent and Electrical Properties of ZnO/GaAs Structures. Journal of the Korean Physical Society, Vol. 42, pp. S357-S360.

Panin G.N.; Kang T.W.; Kim T.W.; Park S.H.; Si S.M.; Ryu Y.S. & Jeon H.C. (2003b). Semiconductor quantum dots created by postgrowth treatment. Physica E 17, pp. 484 –488

Panin G.N., Kang T.W. & Lee H. (2004a). Light emission from the polythiophene derivative/ITO structure under electron beam excitation. Physica E 21, pp. 1074 – 1078.

Panin Gennady N., Kang Tae Won & Lee Haiwon (2004b). Electron beam induced light emission from the polythiophene derivative/ITO structure. phys. stat. sol. (b) 241, No. 12, pp. 2862–2865

Panin G. N., Baranov A. N., Oh Young-Jei & Kang Tae Won (2004c). Luminescence from ZnO/MgO nanoparticle structures prepared by solution techniques. Curr. Appl. Phys. 4, pp. 647-650

Panin G. N.; Park Y. S.; Kang T. W.; Kim T. W.; Wang K. L. & Bao M. (2004d). Self-Assembled GaN Quantum Dots in GaN/AlxGa1-xN Structures Grown by PAMBE. Journal of the Korean Physical Society, Vol. 45, pp. S840-S843.

Panin G. N., Kang T.W., Aleshin A. N., Baranov A. N., Oh Y.-J. & Khotina I. A. (2005a). Electric field switching between blue-green and red cathodoluminescence in poly.4,4′- diphenylene diphenylvinylene. mixed with ZnO:Mg nanoparticles. Appl. Phys. Lett. 86, pp. 113114(3).

Panin G.N., Baranov A.N., Oh Y.-J., Kang T.W. & Kim T.W. (2005b). Effect of thermal annealing on the structural and the optical properties of ZnO/MgO nanostructures. Journal of Crystal Growth 279, pp. 494–500

Panin G. N.; Park Y. S.; Kang T. W.; Kim T. W.; Wang K. L. & Bao M. (2005c). Microstructural and optical properties of self-organized GaN quantum-dot assemblies. J. Appl. Phys., 97, pp. 043527.

Panin Gennady. N.; Baranov Andrey. N.; Kononenko Oleg. V.; Dubonos Sergey. V. & Tae Won Kang (2007a). Resistance Switching Induced by an Electric Field in ZnO:Li, Fe Nanowires. AIP Conf. Proc. 893, pp. 743 -744.

Panin, G.N., Baranov, A.N., Kang, T.W., Kononenko, O.V., Dubonos, S.V., Min S.K. & Kim H.J. (2007b). Electrical and magnetic properties of doped ZnO nanowires. MRS Symp. Proc, 957, pp. 49-54.

Panin G.N.; Baranov A.N.; Kang T.W.; Min S.K. & Kim H.J. (2007c). Spatially-resolved study of magnetic properties of Mn-doped ZnO quantum wires. Journal of the Korean Physical Society 50 (6), pp. 1711-1715.

Panin G. N.; Kim H. J.; Kim S. Y.; Jung J. H.; Kim T. W.; Jeon H. C.; Kang T. W. & Kim M. D. (2007d). Formation and Optical Properties of ZnSe Self-assembled Quantum Dots in Cl-doped ZnSe Thin Films Grown on GaAs (100) Substrates. Solid State Phenomena, 124-126, pp. 567.

Panin Gennady N., Baranov Andrey N., Khotina Irina A. & Kang Tae W. (2008). Luminescent Properties of ZnO/MgO Nanocrystal/Polymer Composite structure. Journal of the Korean Physical Society, Vol. 53, No. 5, pp. 2943-2946.

Pekar S I 1958 Sov. Phys.—JETP 6, pp. 785

Pesika S., Stebe K. J. & Searson P. C. (2003). Determination of the Particle Size Distribution of Quantum Nanocrystals from Absorbance Spectra. Adv. Mater. 15, pp. 1289-1291.

Raghavan S., Hajra J.P., Iyengar G. N. K. & Abraham K.P. (1991). Terminal solid solubilities at 900–1000°C in the magnesium oxide-zinc oxide system measured using a magnesium fluoride solid-electrolyte galvanic cell. Thermochim. Acta 189, pp. 151-158.

Ramakrishna G., G. & Ghosh H.N. (2003). Effect of Particle Size on the Reactivity of Quantum Size ZnO Nanoparticles and Charge-Transfer Dynamics with Adsorbed Catechols. Langmuir 19, pp. 3006-3012.

Reynolds D. C. & Collins T. C. (1969). Excited Terminal States of a Bound Exciton-Donor Complex in ZnO. Phys. Rev. 185, pp. 1099-1103.

Reynolds D. C., Look D. C. & Jogai B. (2001). Fine structure on the green band in ZnO. J. Appl. Phys. 89, pp. 6189-6191.

Riehl N. & Ortman O. Z. (1952) Elektrochem. 60, pp. 149 [in German].

Roessler D.M. & Walker W.C. (1967). Electronic Spectrum and Ultraviolet Optical Properties of Crystalline MgO. Phys. Rev. 159, pp. 733-738.

Rowland G. L., Hosea T. J. C., Malik S., Childs D. & Murray R. (1998). A photomodulated reflectance study of InAs/GaAs self-assembled quantum dots. Appl. Phys. Lett. 73, pp. 3268-3270.

Ryu M. K.; Lee S.; Jang M. S.; Panin G. N. & Kang T. W. Kang (2002). Postgrowth annealing effect on structural and optical properties of ZnO films grown on GaAs substrates by the radio frequency magnetron sputtering technique. J. Appl. Phys., Vol. 92, No. 1, pp. 154-158.

Sakohara S., Ishida M. & Anderson M. A. (1998). Visible Luminescence and Surface Properties of Nanosized ZnO Colloids Prepared by Hydrolyzing Zinc Acetate. J. Phys. Chem. B 102, pp. 10169-10175.

Schmeller A., Hansen W., and Kotthaus J. P. Trinkle G. & Weimann G. (1994) Franz-Keldysh effect in a two-dimensional system. Appl. Phys. Lett. 64 (3), pp. 330-332.

Shalish I., Temkin H., H. & Narayanamurti V. (2004).Size-dependent surface luminescence in ZnO nanowires. Phys. Rev. B 69, pp. 245401(4).

Shannon R.D. (1976). Acta Crystallogr., Sect. A: Cryst. Phys., Diffr., Theor. Gen. Crystallogr. 32, pp. 751.

Sharma A.K., Narayan J., Muth J.F., Teng C.W., Jin C., Kvit A., Kolbas R.M. & Holland O.W. (1999). Optical and structural properties of epitaxial $Mg_xZn_{1-x}O$ alloys. Appl. Phys. Lett. 75, pp. 3327-3329.

Spanhel L. & Anderson M. A. (1991). Semiconductor clusters in the sol-gel process: quantized aggregation, gelation, and crystal growth in concentrated zinc oxide colloids. J. Am. Chem. Soc. 113, pp. 2826-2833.

Shih H. Y.; Chen Y. T.; Huang N. H.; Wei C. M. & Chen Y. F. (2011)Tunable photoluminescence and photoconductivity in ZnO one-dimensional nanostructures with a second below-gap beam. J. Appl. Phys. 109, 103523-1-5.

Sun H.D., Makino T., Tuan N.T., Segawa Y., Tang Z.K., Wong G.K.L., Kawasaki M., Ohtomo A., Tamura K. Koinuma H. (2000). Stimulated emission induced by exciton–exciton scattering in ZnO/ZnMgO multiquantum wells up to room temperature. Appl. Phys. Lett. 77, pp. 4250-4252.

Studenikin S. A., Golego N. & Cocivera M. (1998a). Optical and electrical properties of undoped ZnO films grown by spray pyrolysis of zinc nitrate solution. J. Appl. Phys. 83, pp. 2104-2111.

Studenikin S. A., Golego N. & Cocivera M. (1998b). Fabrication of green and orange photoluminescent, undoped ZnO films using spray pyrolysis. J. Appl. Phys. 84, pp. 2287-2295.

Studenikin S. A., Golego N. & Cocivera M. (1998c). Density of band-gap traps in polycrystalline films from photoconductivity transients using an improved Laplace transform method. J. Appl. Phys. 84, pp. 5001-5004.

Studenikin S. A., Cocivera M., Kellner W. & Pascher H. (2000). Band-edge photoluminescence in polycrystalline ZnO films at 1.7 K. J. Lumin. 91, pp. 223-232.

Studenikin S. A. & M. Cocivera (2002). Time-resolved luminescence and photoconductivity of polycrystalline ZnO films. J. Appl. Phys. 91, pp. 5060-5065.

Takagaki Y., Wiebicke E., Riedel A., Ramsteiner M., Kostial H., Hey R. & Ploog K. H. (2003). Hybrid optical modulator based on surface acoustic waves fabricated using imprint lithography and the epitaxial lift-off technique. Semicond. Sci. Technol. 18, pp. 807-811.

Teke A., Özgür Ü., Doğan S., Gu X. & Morkoç H. (2004). Excitonic fine structure and recombination dynamics in single-crystalline ZnO.Phys. Rev. B 70, pp. 195207(10).

Tokumoto M. S., Pulcinelli S. H., Santilli C. V. & Valérie Briois (2003). Catalysis and Temperature Dependence on the Formation of ZnO Nanoparticles and of Zinc Acetate Derivatives Prepared by the Sol−Gel Route. J. Phys. Chem. B 107, pp. 568-574.

Tomzig E. & Helbig R. (1976). Band-edge emission in ZnO. J. Lumin. 14, pp. 403-415.

Tong Y.H., Liu Y.C., Lu S.X., Dong L., Chen S.J. & Xiao Z.Y. (2004). The Optical Properties of ZnO Nanoparticles Capped with Polyvinyl Butyral. J. Sol– Gel Sci. Technol. 30, pp. 157-161.

Van de Walle C. G. (2001). Defect analysis and engineering in ZnO. Physica B (Amsterdam) 308-310, pp. 899-903.

Van der Horst J.W., Bobbert P.A. & Michels M.A.J. (2002). Electronic and optical excitations in crystalline conjugated polymers. Phys. Rev. B 66, pp. 035206(7).

VanDijken A., Meulenkamp E. A., Vanmaekelbergh D. & Meijerink A. (2000a). The luminescence of nanocrystalline ZnO particles: the mechanism of the ultraviolet and visible emission. J. Lumin. 87-89, pp. 454—456.

Van Dijken A., Meulenkamp E.A., Vanmaekelbergh D. & Meijerink A. (2000b). The Kinetics of the Radiative and Nonradiative Processes in Nanocrystalline ZnO Particles upon Photoexcitation. J. Phys. Chem. B 104, pp. 1715-1723.

Van Dijken A., Makkinje J. & Meijerink A. (2001). The influence of particle size on the luminescence quantum efficiency of nanocrystalline ZnO particles. J. Lumin 92, pp. 323-328.

Vanheusden K.; Seager C. H.; Warren W. L.; Tallant D. R. & Voigt J. A. (1996a). Correlation between photoluminescence and oxygen vacancies in ZnO phosphors. Appl. Phys. Lett. 68, pp. 403-405.

Vanheusden K.; Warren W. L.; Seager C. H.; Tallant D. R. & Voigt J. A. (1996b). Mechanisms behind green photoluminescence in ZnO phosphor powders. J. Appl. Phys. 79, pp. 7983-7990.

Vanheusden K., Seager C. H., Warren W. L., Tallant D. R., Caruso J., Hampden-Smith M. J. & Kodas T. T. (1997). Green photoluminescence efficiency and free-carrier density in ZnO phosphor powders prepared by spray pyrolysis. J. Lumin. 75, pp. 11-16.

Vogel R., Meredith P., Harvey M.D. & Rubinsztein-Dunlop H. (2004). Absorption and fluorescence spectroscopy of rhodamine 6G in titanium dioxide nanocomposites. Spectrochim. Acta Part A 60, pp. 245-249.

Wang X, Ding Y, Summers C J & Wang Z L (2004). Large-Scale Synthesis of Six-Nanometer-Wide ZnO Nanobelts. J. Phys. Chem. B 108, pp. 8773-8777.

Wang H., Xie Ch. & Zeng D. (2005) Controlled growth of ZnO by adding H_2O. J. Cryst. Growth 277, pp. 372-377.

Welter S., Brunner K., Hofstraat J. W. & De Cola L. (2003). Electroluminescent device with reversible switching between red and green emission. Nature, 421, pp. 54-57.

Wong. E. M., Hoertz P. G., Liang C. J., Shi Bai-Ming, Meyer Gerald J. & Searson Peter C. (2001). Influence of Organic Capping Ligands on the Growth Kinetics of ZnO Nanoparticles. Langmuir 17, pp. 8362-8367.

Woo H.S., Czerw R., Webster S. Carroll D. L., Ballato J., Strevens A. E., O'Brien D. & Blau W. J. (2000). Hole blocking in carbon nanotube–polymer composite organic light-emitting diodes based on poly (m-phenylene vinylene-co-2, 5-dioctoxy-p-phenylene vinylene). Appl. Phys. Lett. 77, pp. 1393-1395.

Wood D. L. & Rabinovich E.M. Study of Alkoxide Silica Gels by Infrared Spectroscopy. Appl. Spectrosc. 43, pp. 263-267.

Wu X.L., Siu G.G., Fu C.L. & Ong H.C. (2001). Photoluminescence and cathodoluminescence studies of stoichiometric and oxygen-deficient ZnO films. Appl. Phys. Lett. 78, pp. 2285-2287.

Xia Y, Yang P, Sun Y, Wu Y, Mayers B, Gates B, Yin Y, Kim F & Yan H (2003). One-Dimensional Nanostructures: Synthesis, Characterization, and Applications. Adv. Mater 15, pp. 353-389.

Yang P, Yan H, Mao S, Russo R, Johnson J, Saykally R, Morris N, Pham J, He R & Choi H. J. (2002). Controlled Growth of ZnO Nanowires and Their Optical Properties. Adv. Funct. Mater. 12, pp. 323-331.

Yang C.L., Wang J.N., Ge W.K., Guo L., Yang S.H. & Shen D.Z. (2001). Enhanced ultraviolet emission and optical properties in polyvinyl pyrrolidone surface modified ZnO quantum dots. J. Appl. Phys. 90, pp. 4489-4493.

Yang X. D., Xu Z. Y., Sun Z., Sun B. Q., Ding L., Wang F. Z. & Ye Z. Z. (2006). Recombination property of nitrogen-acceptor-bound states in ZnO. J. Appl. Phys. 99, pp. 046101(3).

Yao B D, Chan Y F & Wang N (2002). Formation of ZnO nanostructures by a simple way of thermal evaporation. Appl. Phys. Lett. 81, pp.757-759.

Yin M, Gu Y, Kuskovsky I L, Andelman T, Zhu Y, Neumark G F & O'Brien S (2004). Zinc Oxide Quantum Rods. J. Am. Chem. Soc. 126, pp. 6206-6207.

Ying J.Y., Benziger J.B. & Navrotsky A. (1993). Structural Evolution of Alkoxide Silica Gels to Glass: Effect of Catalyst pH. J. Am. Ceram. Soc. 76, pp. 2571-2582.

Zhang B. P., Binh N. T., Segawa Y., Wakatsuki K. & Usami N. (2003). Optical properties of ZnO rods formed by metalorganic chemical vapor deposition. Appl. Phys. Lett. 83, pp. 1635(3).

Zhang S. B., Wei S.-H. & Zunger A. (2001). Intrinsic n-type versus p-type doping asymmetry and the defect physics of ZnO. Phys. Rev. B 63, pp. 075205(7).

Zhang S. K., Santos P. V. & Hey R. (2001). Photoluminescence modulation by high-frequency lateral electric fields in quantum wells. Appl. Phys. Lett. 78, pp. 1559-1561.

Zhang X H, Xie S Y, Jiang Z Y, Xie Z X, Huang R B, Zheng L S, Kang J Y & Sekiguchi T. (2003). Microwave plasma growth and high spatial resolution cathodoluminescent spectrum of tetrapod ZnO nanostructures. J. Solid State Chem. Chem. 173, pp. 109-113.

Zhao Q.X., Klason P., Willander M., Zhong H.M., Lu W. & Yang J.H. (2005). Deep-level emissions influenced by O and Zn implantations in ZnO. Appl. Phys. Lett. 87, pp. 211912(3).

Zimmermann S.; Govorov A. O.; Hansen W.; Kotthaus J. P.; Bichler M. & Wegscheider W. (1997). Lateral superlattices as voltage-controlled traps for excitons, Phys. Rev. B 56, pp. 13414–13421

Zimmermann S.; Schedelbeck G.; Govorov A. O.; Wixforth A.; Kotthaus J. P.; Bichler M.; Wegscheider W.; & Abstreiter G. (1998). Spatially resolved exciton trapping in a voltage-controlled lateral Superlattice. Appl. Phys. Lett., Vol. 73, No. 2, pp. 154-156.

Zimmermann S.; Wixforth A.; Kotthaus J. P.; Wegscheider W.; & Bichler M. (1999). A Semiconductor-Based Photonic Memory Cell. Science 283, pp. 1292-1295.

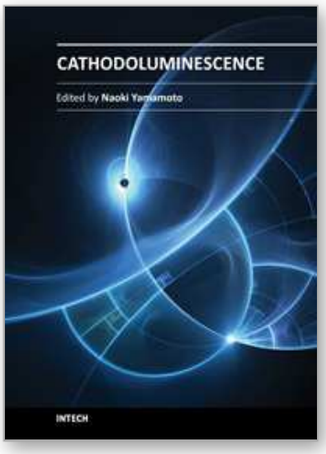

Cathodoluminescence

Edited by Dr. Naoki Yamamoto

ISBN 978-953-51-0362-2
Hard cover, 324 pages
Publisher InTech
Published online 28, March, 2012
Published in print edition March, 2012

Cathodoluminescence (CL) is a non-destructive technique to characterize optical and electronic properties of nanostructures in many kinds of materials. Major subject is to investigate basic parameters in semiconductors, impurities in oxides and phase determination of minerals. CL gives information on carrier concentration, diffusion length and life time of minority carriers in semiconductors, and impurity concentration and phase composition in composite materials. This book involves 13 chapters to present the basics in the CL technique and applications to particles, thin films and nanostructures in semiconductors, oxides and minerals. The chapters covered in this book include recent development of CL technique and applications to wide range of materials used in modern material science.

How to reference

In order to correctly reference this scholarly work, feel free to copy and paste the following:

G.N. Panin (2012). Multicolor Luminescence from Semiconductor Nanocrystal Composites Tunable in an Electric Field, Cathodoluminescence, Dr. Naoki Yamamoto (Ed.), ISBN: 978-953-51-0362-2, InTech, Available from: http://www.intechopen.com/books/cathodoluminescence/multicolor-luminescence-from-semiconductor-nanocrystal-composites-tunable-in-an-electric-field

INTECH
open science | open minds

InTech Europe
University Campus STeP Ri
Slavka Krautzeka 83/A
51000 Rijeka, Croatia
Phone: +385 (51) 770 447
Fax: +385 (51) 686 166
www.intechopen.com

InTech China
Unit 405, Office Block, Hotel Equatorial Shanghai
No.65, Yan An Road (West), Shanghai, 200040, China
中国上海市延安西路65号上海国际贵都大饭店办公楼405单元
Phone: +86-21-62489820
Fax: +86-21-62489821